

Differences in Flexibility Underlie Functional Differences in the Ras Activators Son of Sevenless and Ras Guanine Nucleotide Releasing Factor 1

Tanya S. Freedman,^{1,8} Holger Sondermann,^{1,9} Olga Kuchment,² Gregory D. Friedland,^{3,4,5} Tanja Kortemme,^{4,5} and John Kuriyan^{1,2,6,7,*}

¹Department of Molecular and Cell Biology, California Institute for Quantitative Biomedical Research

²Department of Chemistry

University of California, Berkeley, Berkeley, CA 94720, USA

³Graduate Group in Biophysics

⁴Department of Biopharmaceutical Sciences

⁵California Institute for Quantitative Biomedical Research

University of California, San Francisco, San Francisco, CA 94143, USA

⁶Howard Hughes Medical Institute, University of California, Berkeley, Berkeley, CA 94720, USA

⁷Physical Biosciences Division, Lawrence Berkeley National Laboratory, Berkeley, CA 94720, USA

⁸Present address: Howard Hughes Medical Institute and Department of Medicine, University of California, San Francisco, San Francisco, CA 94143, USA

⁹Present address: Department of Molecular Medicine, College of Veterinary Medicine, Cornell University, Ithaca, NY 14853, USA

*Correspondence: kuriyan@berkeley.edu

DOI 10.1016/j.str.2008.11.004

SUMMARY

The Ras-specific nucleotide exchange factor Son of sevenless (Sos) is inactive without Ras bound to a distal allosteric site. In contrast, the catalytic domain of Ras guanine nucleotide releasing factor 1 (RasGRF1) is active intrinsically. By substituting residues from RasGRF1 into Sos, we have generated mutants of Sos with basal activity, partially relieved of their dependence on allosteric activation. We have performed molecular dynamics simulations showing how Ras binding to the allosteric site leads to a bias toward the active conformation of Sos. The trajectories show that Sos fluctuates between active and inactive conformations in the absence of Ras and that the activating mutations favor conformations of Sos that are more permissive to Ras binding at the catalytic site. In contrast, unliganded RasGRF1 fluctuates primarily among active conformations. Our results support the premise that the catalytic domain of Sos has evolved an allosteric activation mechanism that extends beyond the simple process of membrane recruitment.

INTRODUCTION

The nucleotide exchange factors Son of sevenless (Sos) and Ras guanine nucleotide releasing factor 1 (RasGRF1) activate Ras by converting GDP-bound Ras to GTP-bound Ras. A helical hairpin motif in the catalytic domain of Sos binds to and disrupts the nucleotide binding site of Ras, thereby promoting nucleotide release and exchange (Boriack-Sjodin et al., 1998; Vetter and Wittinghofer, 2001; Figure 1A). Ras then binds GTP, after which it can activate signaling proteins that control cell growth, differ-

entiation, and survival (Herrmann and Nassar, 1996). Ras is a potent oncogene, and inappropriate activation of Ras has been implicated in the majority of human cancers (Coleman et al., 2004; Hanahan and Weinberg, 2000; Schubert et al., 2007). The nucleotide exchange activity of Sos and RasGRF1 must therefore be tightly regulated to prevent cellular transformation by constitutively high levels of activated Ras (Egan et al., 1993; Herrmann and Nassar, 1996). Sos itself has been shown to transform cells (Egan et al., 1993), and hyperactivated forms of Sos have been linked to Noonan syndrome, a developmental disease that stems from dysregulation of the Ras pathway (Roberts et al., 2007; Tartaglia et al., 2007).

Two domains of Sos are required for Ras-specific nucleotide exchange activity: a Cdc25 domain named for the activator of Ras in yeast and a Ras exchanger motif (Rem) domain (Figure 1A). The active site is located entirely within the Cdc25 domain and consists of a hydrophobic pocket for anchoring Ras and the helical hairpin motif that stimulates nucleotide release (Boriack-Sjodin et al., 1998; Freedman et al., 2006). Sos is activated by Ras binding to an allosteric site that bridges the Rem and Cdc25 domains, and we refer to the Ras molecule bound to the allosteric site as “allosteric Ras” (Margarit et al., 2003). In a crystal structure of the isolated Rem and Cdc25 domains of Sos, the helical hairpin is pivoted toward the central core of the Cdc25 domain and occludes the catalytic site (Freedman et al., 2006; Figure 1). Allosteric Ras binding pivots the Rem domain outward from the stable core of the Cdc25 domain, repositioning the helical hairpin and opening the catalytic site for Ras binding (Freedman et al., 2006; Margarit et al., 2003).

In a structure of a Sos construct that includes the N-terminal Dbl homology (DH) and pleckstrin homology (PH) domains as well as the Rem and Cdc25 domains (Sos^{DPC}), the DH domain blocks the allosteric Ras binding site (Sondermann et al., 2004). As expected, the active site is occluded by the helical hairpin in this structure, and the Rem domain is pivoted away from the conformation in which it interacts with allosteric Ras

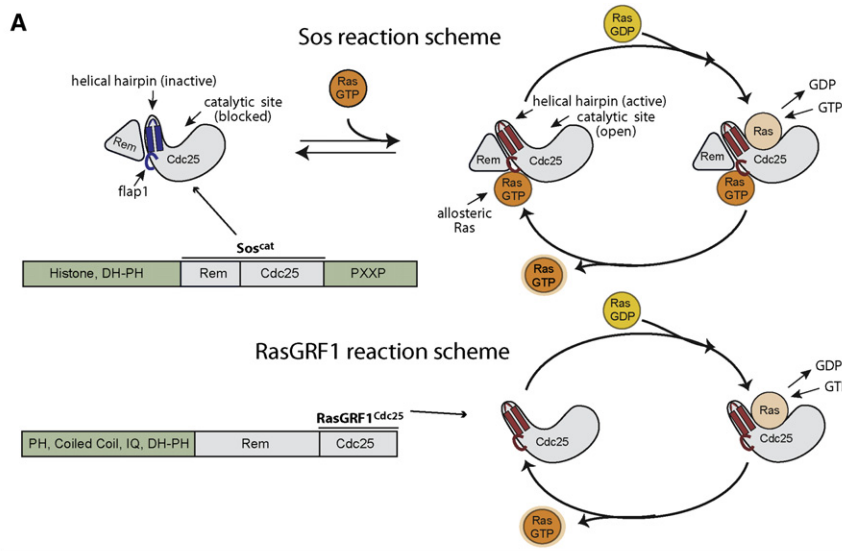
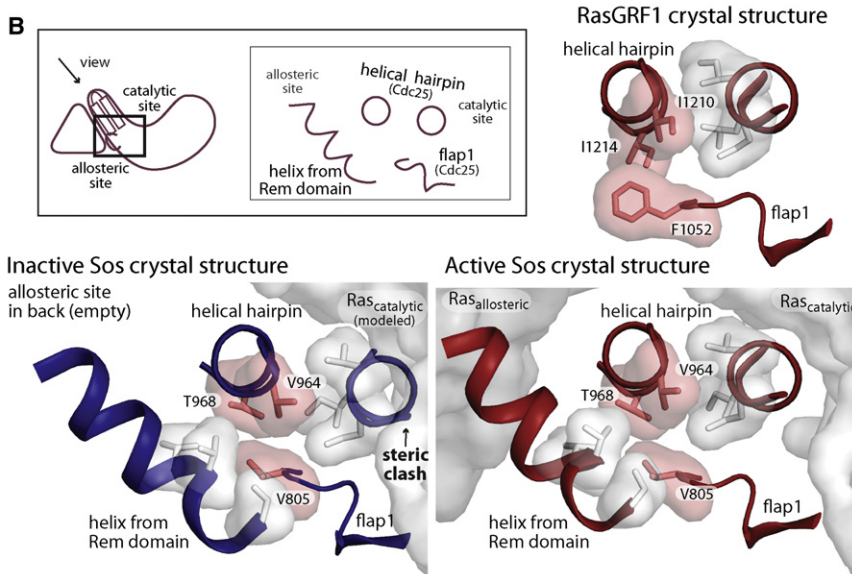


Figure 1. Comparison of Sos and RasGRF1
(A) Schematic diagram comparing the activation of Ras by Sos and RasGRF1.

(B) Interface between Ras and nucleotide exchange factors, and residues mutated in this study. A view down the helical hairpin of Sos highlights the conformational change that occurs upon Ras binding to the allosteric site. The Ras molecule is modeled into the structure of inactive Sos (PDB ID code 2II0; Freedman et al., 2006) from the crystal structure of active Sos (PDB ID code 1NVV; Margarit et al., 2003). When Ras binds to the allosteric site of Sos, the Rem domain is pivoted downward to maintain this interaction. The helical hairpin is also pivoted outward to open the catalytic site. Residues V805, V964, and T968, which comprise an interface between the Rem domain, flap1, and the helical hairpin, are highlighted in pink. RasGRF1 (PDB ID code 2IJE; Freedman et al., 2006) assumes an active conformation in the absence of bound Ras.



on a comparison of crystal structures of active Sos, inactive Sos, and RasGRF1, we have postulated that RasGRF1 is held in an active conformation by bulky residues that comprise an interface between the helical hairpin and an extension of the Cdc25 domain called flap1 (Figure 1). In addition, we had used Monte Carlo simulations to predict whether swapping residues in the sequences of RasGRF1 and Sos would stabilize the observed backbone conformations (Freedman et al., 2006). In these simulations, a cluster of three mutations was predicted to stabilize the active conformation of Sos, but not the inactive conformation. The corresponding positions in

RasGRF1 remained unaltered during the Monte Carlo simulations, suggesting that the wild-type sequence of RasGRF1 is superior for stabilizing the active conformation of both RasGRF1 and Sos. These residues (F1052, I1210, and I1214 in RasGRF1 versus V805, V964, and T968 in Sos) lie in the interface formed by the helical hairpin and flap1 in the Cdc25 domain (Figure 1B), and we suggested that the bulkier residues from RasGRF1 could be important for maintaining the active conformation (Freedman et al., 2006). Here we show that substituting one or more residues from flap1 and from the helical hairpin of RasGRF1 into Sos substantially increases the basal activity of Sos in the absence of allosteric Ras binding. We use molecular dynamics simulations to investigate how these substitutions alter the behavior of Sos and show that RasGRF1 and Sos sample different sets of conformations in the absence of Ras binding. In addition, we find that inactive Sos fluctuates between the inactive and active conformations.

(Sondermann et al., 2004). The N-terminal histone domain confers an additional level of autoinhibition to Sos (Gureasko et al., 2008) by binding to the PH-Rem domain linker and reinforcing the position of the DH domain (Sondermann et al., 2005; O. Kuchment, J. Gureasko, and J.K., unpublished data). The histone domain may also prevent a conformational change that opens the allosteric site upon phosphatidylinositol bisphosphate binding to the PH domain (Gureasko et al., 2008). Thus, a significant portion of the regulatory apparatus of Sos is devoted to blocking the allosteric site, and this autoregulation relies on the intrinsic inactivity of the catalytic domain.

In contrast to Sos, the Cdc25 domain of RasGRF1 has intrinsic activity without the Rem domain and without an allosteric effector being bound (Cocchetti et al., 1995; Freedman et al., 2006; Lenzen et al., 1995; Figure 1A). The crystal structure of the isolated Cdc25 domain of RasGRF1 shows that the helical hairpin is pivoted outward from the core of the Cdc25 domain, leaving the catalytic site open (Freedman et al., 2006). Based

on a comparison of crystal structures of active Sos, inactive Sos, and RasGRF1, we have postulated that RasGRF1 is held in an active conformation by bulky residues that comprise an interface between the helical hairpin and an extension of the Cdc25 domain called flap1 (Figure 1). In addition, we had used Monte Carlo simulations to predict whether swapping residues in the sequences of RasGRF1 and Sos would stabilize the observed backbone conformations (Freedman et al., 2006). In these simulations, a cluster of three mutations was predicted to stabilize the active conformation of Sos, but not the inactive conformation. The corresponding positions in

RESULTS

Mutations that Activate Sos

There are several mechanisms that contribute to Sos activation upon recruitment to the membrane: allosteric activation by membrane-localized Ras, tethering at the membrane through the allosteric site, and release of autoinhibition by lipid binding (Gureasko et al., 2008). To investigate the properties intrinsic to the catalytic domains of Sos that lead to its dependence on allosteric activation, we chose to measure activity in solution rather than at the membrane, and at low concentrations of both Ras and Sos. Thus, we eliminated the effects of crowding at the membrane (Gureasko et al., 2008) and minimized allosteric activation by Ras (Freedman et al., 2006).

We tested the effects of substituting the bulkier residues in the flap1/helical hairpin interface of RasGRF1 into Sos^{cat}, a construct of Sos that includes the Rem and Cdc25 domains (Freedman et al., 2006; Margarit et al., 2003; Figure 1A). We were unable to express a Rem-Cdc25 construct of RasGRF1 and so restricted our analysis to the Cdc25 construct, which is active. We monitored nucleotide exchange activity as reflected in the decrease in emission intensity of a fluorescent GDP analog, mant-dGDP, upon release from Ras (Freedman et al., 2006; Guo et al., 2005; Lenzen et al., 1995, 1998).

As observed previously, Sos (Sos^{cat}, unless otherwise specified) has very little basal activity in the absence of allosteric Ras binding, whereas the rate of nucleotide release stimulated by RasGRF1 (a construct called RasGRF1^{Cdc25} that includes only the Cdc25 domain) is at least 10-fold higher than that for Sos under the same conditions (Freedman et al., 2006; Figures 2A and 2B). With a single mutation (T968I) in the helical hairpin of Sos, denoted Sos(TI), ~30% of the activity of RasGRF1 is achieved. A triple mutant with T968I and V964I in the helical hairpin and V805F in flap1, called Sos(VFVITI), has ~45% of the basal activity of RasGRF1, at least a 5-fold increase over wild-type Sos (Figure 2B). A double mutant (V805F+T968I) and the variant T968L also increase the basal activity of Sos (see Figure S1A available online).

To ensure that these measured rate enhancements result from a true increase in basal activity and not, for instance, from increased affinity for allosteric Ras, we also tested these mutations in combination with the mutation W729E in the Rem domain of Sos. The W729E mutation blocks Ras binding to the allosteric site, and would therefore cause a decrease in activity if the original gain was attributable to substrate binding to the allosteric site (Margarit et al., 2003). All of the activated mutants showed similar behavior in backgrounds of wild-type Sos and of Sos with the W729E mutation (Figure S1A), and thus we conclude that substituting residues in the helical hairpin and flap1 of Sos partially relieves Sos of its dependence on allosteric activation.

Although both Sos(TI) and Sos(VFVITI) are activated relative to wild-type Sos, they differ in their ability to be further stimulated by allosteric Ras binding. We measured the effect of allosteric Ras binding on Sos activity by performing nucleotide exchange reactions with different concentrations of Ras^{Y64A}, a variant of Ras that binds to the allosteric site but not to the catalytic site of Sos (Hall et al., 2001; Margarit et al., 2003). The Ras^{Y64A} variant is effective as an allosteric stimulator of Sos, but it does not compete with wild-type Ras for the active site of Sos.

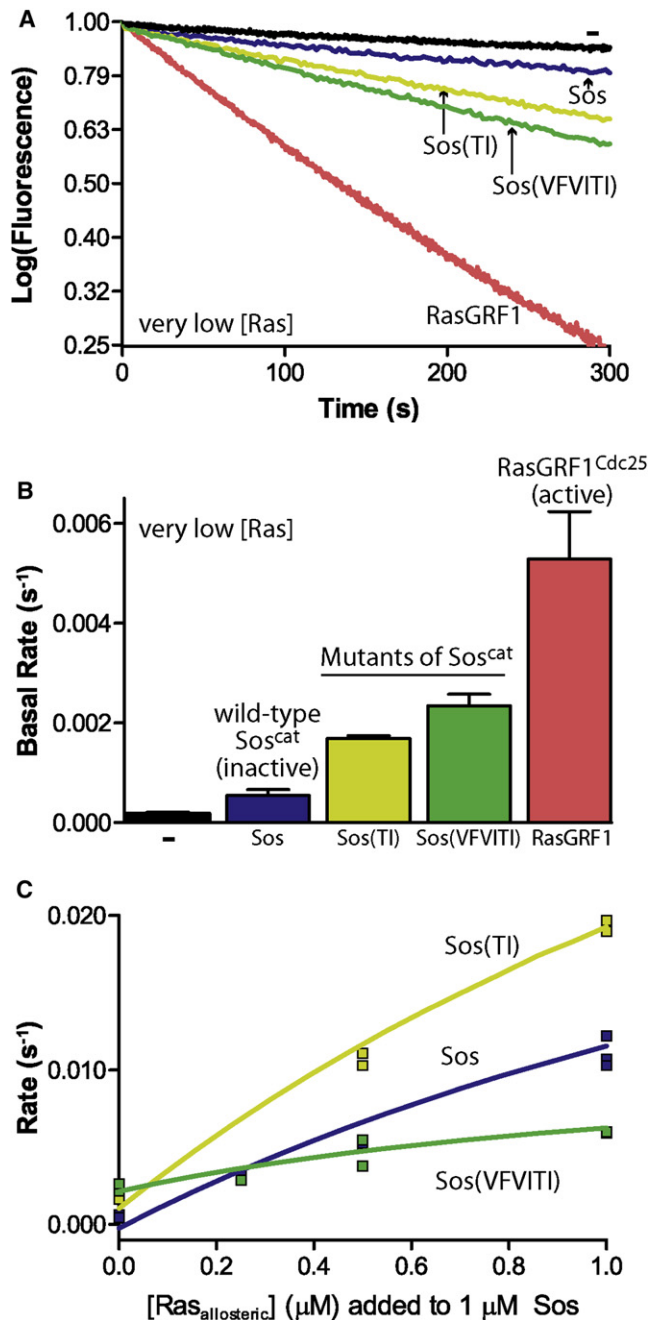
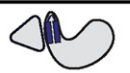
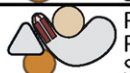


Figure 2. Engineering Intrinsic Activity into Sos

(A and B) Nucleotide release assays show that RasGRF1 (Cdc25 domain) has a high basal activity compared to Sos (Rem and Cdc25 domains). Substituting residues from the flap1/helical hairpin interface of RasGRF1 into Sos increases the basal activity of Sos. The error bars represent the standard deviation of the fit rates of at least three independent experiments.

(C) Two mutants have different responses to allosteric Ras binding. The single mutant T968I (Sos(TI)) is more active than wild-type Sos at all concentrations of Ras^{Y64A}, a variant of Ras that binds selectively to the allosteric site. The triple mutant V805F+V964I+T968I (Sos(VFVITI)) has the highest basal activity, but fails to respond to allosteric Ras binding and has a dramatically impaired maximal activity.

Table 1. Molecular Dynamics Simulations

Simulation	Starting Structure	Molecules Included	Mutations	# Trajectories (7 ns each)
GRF		RasGRF1	none	6
Ras•Sos ^{Active} •Ras		Ras ^{cat} Ras ^{allo} Sos	none	1
Ras•Sos ^{Active}		Ras ^{cat} Ras ^{allo} Sos	none	6
Sos ^{Active}		Ras ^{cat} Ras ^{allo} Sos	none	7
Sos ^{Inactive}		Sos	none	8
Sos(TI) ^{Inactive}		Sos	T968I	6
Sos(VFVITI) ^{Inactive}		Sos	V805F+V964I+T968I	6
Sos(TI) ^{Active}		Ras ^{cat} Ras ^{allo} Sos	T968I	6
Sos(VFVITI) ^{Active}		Ras ^{cat} Ras ^{allo} Sos	V805F+V964I+T968I	6

The starting structure for RasGRF1 comes from the crystal structure of RasGRF1^{Cdc25} (PDB ID code 2IJE; Freedman et al., 2006), the starting structure for active Sos comes from the crystal structure of Sos^{cat} (PDB ID code 1NVV; Margarit et al., 2003) with two bound Ras molecules, and the starting structure for inactive Sos comes from the crystal structure of apo-Sos^{cat} (PDB ID code 2IIO; Freedman et al., 2006). Mutations were created in the wild-type crystal structures using PyMOL (DeLano, 2002). Ras^{cat}, catalytic-site Ras; Ras^{allo}, allosteric-site Ras; Sos, Sos^{cat} (Rem + Cdc25 domains); RasGRF1, RasGRF1^{Cdc25}.

At each concentration of Ras^{Y64A}, Sos(TI) is more active than wild-type Sos, showing that Sos(TI) is sensitive to allosteric activation by Ras. Sos(VFVITI) is, however, almost unresponsive to titration of Ras^{Y64A}, suggesting that its sensitivity to allosteric activation is impaired (Figure 2C; Figures S1B and S1C). These differences in sensitivity to allosteric activation cannot be explained by changes in the affinity of the allosteric site for Ras^{Y64A}; Sos(VFVITI) actually has increased affinity, whereas the affinity of Sos(TI) for Ras^{Y64A} is comparable to that of wild-type Sos (Figure S1D). Although both mutants have increased basal activity, the mutation in Sos(TI) does not interfere with its allosteric activation, whereas the mutations in Sos(VFVITI) impair allosteric activation. This implies that these two mutants have different mechanisms for achieving basal activity, as discussed later.

Molecular Dynamics Simulations of RasGRF1, Sos, and Sos Mutants

We generated a series of unbiased molecular dynamics trajectories (Dodson et al., 2008; Karplus and Kuriyan, 2005) for Sos, RasGRF1, and the activated mutants of Sos on the nanosecond timescale (Table 1). The starting structure for each trajectory was generated from crystal structures of RasGRF1, of active Sos with bound allosteric Ras and catalytic-site Ras, and of inactive Sos (Freedman et al., 2006; Margarit et al., 2003). We also modeled the activating mutations into the active or inactive crystal struc-

ture of Sos. We used the AMBER software package (Pearlman et al., 1995) to place the protein chain(s) of each modified starting structure into a box of water in solution with 150 mM sodium chloride and counterions to bring the net charge to zero. Independent trajectories of 7 ns each were generated, with at least six trajectories for each starting structure. All of the trajectories were stable throughout, as determined by visual analysis and calculation of the root-mean-square deviation (rmsd) with respect to the starting structures (Figure S2). The trajectories were analyzed extensively using various methods, such as crosscorrelation matrices and by calculating normal modes (principal component analysis of the fluctuations). The most informative analysis, however, proved to be simple comparisons of the structures of the proteins as the trajectories evolved, and we therefore restrict our discussion to these structural comparisons. The timescales for the inactive-to-active transitions in Sos and RasGRF1 are not known, but are likely to be in the microsecond to millisecond range. Our simulations do not provide direct information on the nature of the transitions, but rather provide information about the behavior of these proteins when in one state of activation or the other.

Structures from points along the trajectories were analyzed after alignment on the core of the Cdc25 domain, which does not differ significantly in the active and inactive conformations of Sos (C_{α} rmsd = 0.3 Å). In all the simulations, these residues in the core of the Cdc25 domain remain close to their starting

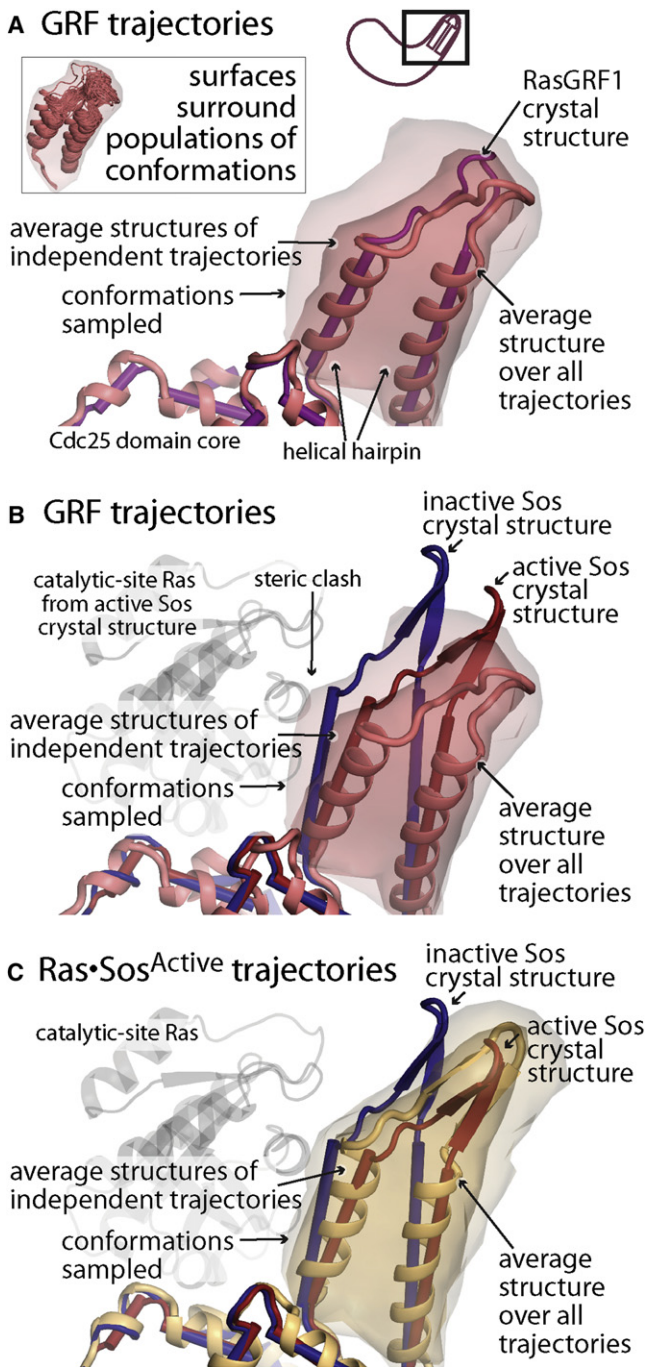


Figure 3. Conformation of the Helical Hairpin in Molecular Dynamics Trajectories of Active Sos and RasGRF1

(A) The average conformation over the six GRF trajectories is similar to that observed in the crystal structure of RasGRF1 (pink and purple cartoons, respectively). The light surface reflects the range of sampled conformations, including the average structures for 500 ps windows over all the trajectories and eight instantaneous structures representing the extremes of conformation with respect to active and inactive Sos (determined individually by C_{α} rmsd of the helical hairpin or the Rem domain with respect to comparable regions of active Sos or of inactive Sos. The instantaneous structures with the highest and lowest rmsd values for both regions with respect to both crystal structures represent the diversity of conformations achieved during the trajectories). The dark surface surrounds the six structures that represent the average confor-

positions (average C_{α} rmsd with respect to the starting structures for the residues in the Cdc25-domain core ranges from 0.5 to 0.7 Å for all sets of trajectories; Figure S2). We then compared the conformations of the helical hairpin and the motifs in the Rem domain that interact with allosteric Ras, which differ in crystal structures of active and inactive Sos by C_{α} rmsd values of 3.3 and 7.8 Å, respectively. Over the course of the trajectories, these residues change position to a greater extent than the residues in the core of the Cdc25 domain. In the following analysis, we refer to these residues in the helical hairpin and Rem domain as indicators of conformational change. The average C_{α} rmsd of the helical hairpin residues with respect to the starting structure (see [Experimental Procedures](#)) varies from 1.6 to 2.9 Å over all sets of trajectories (Figure S3). The average C_{α} rmsd of the Ras-interacting residues in the Rem domain varies from 2.0 to 7.3 Å over all sets of trajectories (Figure S4).

RasGRF1 and Ras-Bound Sos Are Stable in the Active Conformation

The molecular dynamics trajectories indicate that the isolated Cdc25 domain of RasGRF1 stably maintains the active conformation. The following discussion is based on an analysis of six independent trajectories of 7 ns each (denoted “GRF”; Table 1), but one of these simulations was carried out to 19 ns and yielded consistent results throughout. After alignment on the relatively rigid core of the Cdc25 domain, the mean position of the helical hairpin overall is similar to that in individual trajectories starting from the crystal structure of RasGRF1 (Figure 3A, cartoons). The average position of the helical hairpin is also similar in each independent simulation (Figure 3A, dark surface), but the helical hairpin is flexible compared to the core of the Cdc25 domain, sampling a range of positions around the average conformation (Figure 3A, light surface). As in the crystal structure of RasGRF1 (Freedman et al., 2006), the average position of the helical hairpin in the GRF trajectories is closer to its position in active Sos than to that in inactive Sos (Figure 3B, cartoons). The trajectories show that GRF does, on rare occasions, sample conformations similar to the crystal structure of inactive Sos, where the helical hairpin would clash with Ras at the active site (when Ras is modeled into the active site from its position in the crystal structure of Ras-bound Sos; Figure 3B).

Trajectories of active Sos with Ras molecules bound both at the allosteric and catalytic sites (Ras•Sos^{Active}•Ras; Table 1) show, not surprisingly, that the helical hairpin remains close to the active conformation (Figure S5, first panel). Likewise, trajectories for Sos with Ras bound only to the allosteric site (Ras•Sos^{Active}; Table 1) maintain average helical hairpin conformations similar to that in the crystal structure of active Sos (Figure 3C, cartoon, dark surface). The helical hairpin in the simulations of Ras•Sos^{Active}, however, has considerably less freedom to fluctuate toward the inactive conformation of Sos

mation of each individual simulation and thus reflects the heterogeneity among different simulations.

(B) In the GRF simulations, the helical hairpin is in a position more similar to active Sos (red) than to inactive Sos (blue). The helical hairpin samples conformations, however, that would clash with Ras bound to the catalytic site. (C) Ras•Sos^{Active} simulations are more limited in the range of conformations sampled by the helical hairpin, avoiding clashes with Ras at the catalytic site.

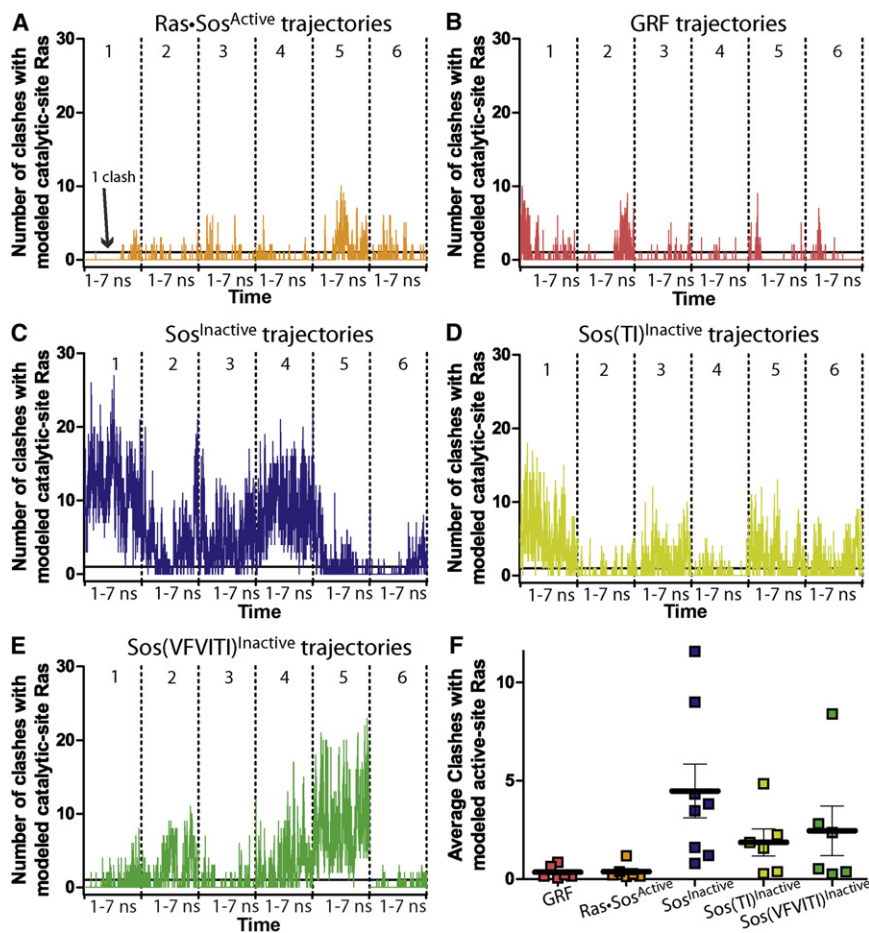


Figure 4. Active-Site Occlusion by the Helical Hairpin during the Simulations

(A–E) The number of clashes (C_{α} - C_{α} contacts closer than 2.2 Å) between the helical hairpin and a Ras molecule modeled into the active site is counted every 10 ps along the trajectory of each simulation. The solid line indicates one backbone clash between the helical hairpin and catalytic-site Ras. Six simulations are concatenated in each panel, and the dotted lines represent the boundaries between them.

(F) The average number of clashes over each trajectory over time is plotted as a square. Points with similar y axis values are spaced horizontally for clarity. The horizontal bars represent the overall average number of clashes for all simulations. According to an ANOVA analysis, RasGRF1, Ras•Sos^{Active}•Ras (see Figure S6), and Ras•Sos^{Active} simulations are not significantly different in their extents of active-site occlusion. All other pairs of simulations in this figure have significantly different numbers of clashes between the helical hairpin and active-site Ras ($p > .0001$).

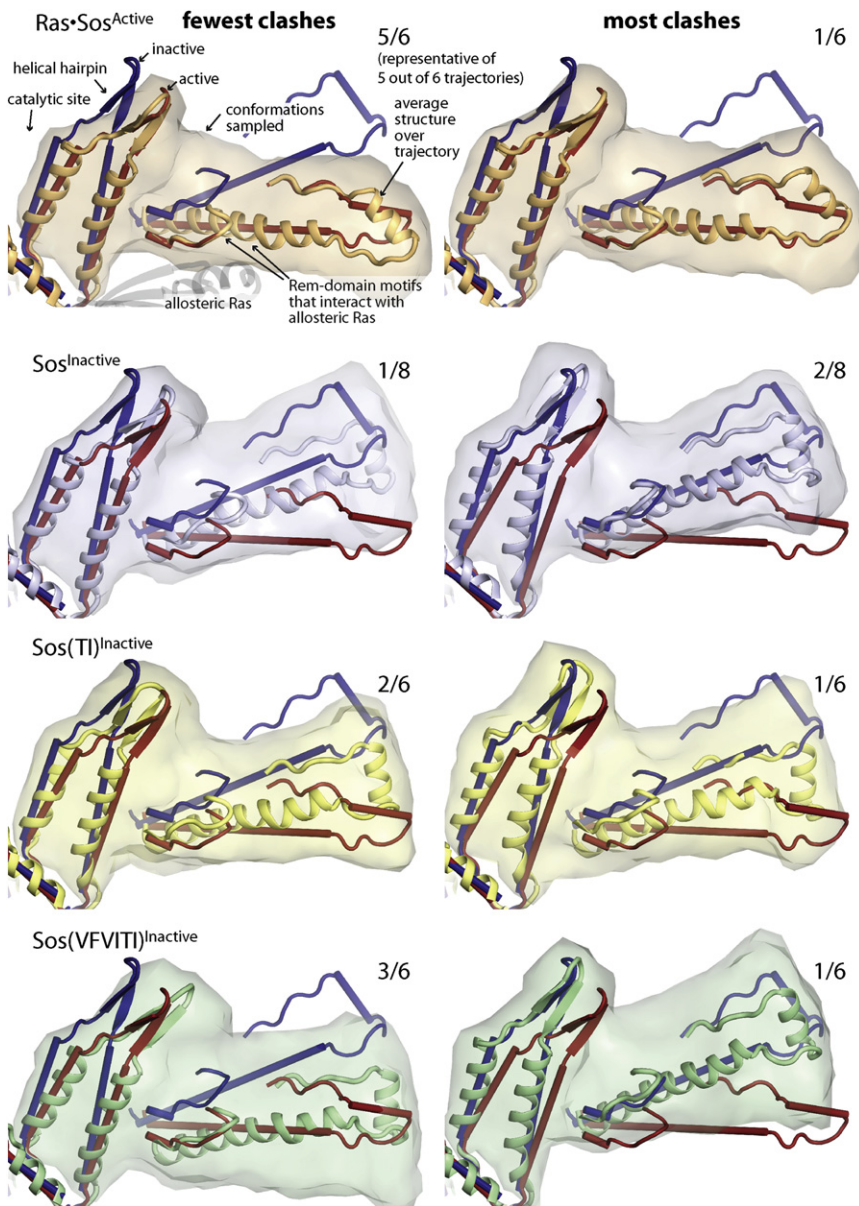
than seen in the GRF simulations and never approaches a conformation like inactive Sos (Figure 3C, light surface). This narrowed range of conformations is most likely due to the bound allosteric Ras molecule, which constrains the helical hairpin of Sos in the active conformation.

To provide a more quantitative metric for the extent to which the trajectories sample inactive conformations such as the one observed in the crystal structure of isolated Sos^{cat} (Freedman et al., 2006), we calculated the number of close contacts between the helical hairpin and a Ras molecule bound at the catalytic site (see Experimental Procedures for details of this modeling). By this metric, trajectories for Ras•Sos^{Active} do occasionally fluctuate into conformations that partially occlude the active site (Figure 4A). This analysis relies on a rigidly docked Ras molecule at the catalytic site and does not account for complementary motions in Ras and Sos. Thus, for the Ras•Sos^{Active}•Ras trajectory, which has Ras bound at the catalytic site of Sos for the duration of the simulation without steric clash, this contact metric also reports occasional clashes (Figure S6, first panel). We therefore consider this low level of clashes to be characteristic of the active conformation. It should be emphasized, however, that because the reference Ras molecule is rigidly docked, this metric is only a rough indicator of occlusion of the active site.

In this respect, the Ras•Sos^{Active}•Ras trajectories and the Ras•Sos^{Active} trajectories are not significantly different (averaging 0.2 ± 0.5 clashes for any instantaneous structure over the trajec-

tory of Ras•Sos^{Active}•Ras and 0.4 ± 1.0 clashes per instantaneous structure over the six trajectories of Ras•Sos^{Active}; Figure 4F; Figure S6). Therefore, when the average number of these clashes per instantaneous structure over the duration of a simulation is less than 1, we conclude that the active site is not occluded. GRF also fluctuates into conformations that occlude the active site (Figure 4B), but as with Ras•Sos^{Active}, these simulations have, on average, less than 1 clash per instantaneous structure over all the trajectories (Figure 4F; 0.3 ± 1.0 clashes per instantaneous structure). This confirms that both RasGRF1 and Sos maintain open active-site conformations.

The Rem domain is important for the coupling of allosteric Ras binding to the activation of Sos (Freedman et al., 2006; Hall et al., 2001). For analysis of the conformational changes of the Rem domain, we examined the structural motifs that interact with allosteric Ras, which change in a concerted manner upon activation of Sos (Figure 5A). We define the active conformation of the Rem domain as the conformation observed in the crystal structure of Ras-bound Sos (Margarit et al., 2003), in which these motifs are pivoted so as to interact with allosteric Ras (Figure 5A, red). These portions of the Rem domain are pivoted into nonproductive positions in the crystal structure of inactive Sos (Figure 5A, blue; Freedman et al., 2006). The trajectory for Ras•Sos^{Active}•Ras (Figure S7A) shows that, like that of the helical hairpin, the average position of the Rem domain over all the simulations is very close to that seen in the crystal structure of active Sos. Similarly, the Rem domain consistently maintains the active conformation in the Ras•Sos^{Active} trajectories (Figure 5A). Moreover, the average root-mean-square (rms) fluctuation, which reveals the average degree of motion over each simulation, is low for the Rem domain in the simulations of Ras•Sos^{Active} (Figure 6A).



This is consistent with the model that allosteric Ras binding couples the Rem domain and the helical hairpin, holding both in an active conformation.

In the Absence of Ras, the Helical Hairpin of Sos Fluctuates between Active and Inactive Conformations

We also generated molecular dynamics trajectories for Sos without any bound Ras, starting from the inactive crystal structure (Sos^{Inactive}; Table 1). Unlike the trajectories for Ras•Sos^{Active} and GRF, the independent trajectories for Sos^{Inactive} vary significantly (Figure 6B, overlaid structures; Figure 4F). Thus, the following analysis begins with a discussion of individual trajectories that represent different populations within the set. Sos^{Inactive} trajectories show dramatic active-site occlusion (Figures 4C and 4F; an average of 4.5 clashes per instantaneous structure for Sos^{Inactive}). Compared to Ras•Sos^{Active}, Sos^{Inactive} trajectories

Figure 5. Rem Domain and Helical Hairpin Conformations in Sos Trajectories

The crystal structures of active and inactive Sos are depicted in red and blue, respectively. In the left column is the result of one trajectory (of the type indicated) with the lowest average number of clashes with Ras modeled into the active site. In the right column is depicted the trajectory with the greatest number of clashes. The fraction of related simulations represented by each panel is indicated (for instance, 5/6 means that five simulations of the six performed have a similar degree of active-site occlusion to the one shown). The light surface reflects the range of conformations sampled within the simulation, including the conformations with highest and lowest helical-hairpin and Rem-domain rmsd with respect to active and inactive Sos as well as the average structures for every 500 ps of the simulation. Simulations not shown have intermediate degrees of active-site occlusion and are depicted in Figures S7 and S8.

have high rms fluctuation values, especially in the Rem domain (Figure 6B, colors). In fact, the average position of the helical hairpin in one Sos^{Inactive} trajectory closely resembles the one found in active Sos (Figure 5B, left), whereas in other simulations it more closely resembles the position in inactive Sos or intermediate conformations between the two (Figure 5B, right; Figure S8A). Although the helical hairpin samples the full range of conformations from inactive to active in the Sos^{Inactive} simulations, the Rem domain never samples the active conformation (Figure 5B, surface).

The limited ability of the Rem domain of Sos to switch between the active and inactive conformations is evident also in the trajectories of unliganded Sos starting from the active conformation (Sos^{Active}; Table 1). Unlike the Ras•Sos^{Active} trajectories, the Sos^{Active} trajectories show the helical hairpin fluctuating into conformations that occlude the active site (Figure S6). However, the average conformation of the helical hairpin over the Sos^{Active} trajectories remains more like that in active Sos than in the Sos^{Inactive} trajectories (Figures S5 and S7B). This bias toward the starting structure is surprising given the fact that the helical hairpin samples the active and inactive positions multiple times during several of the simulations. The discrepancy suggests that although the helical hairpin may be flexible, the Rem domain has not yet broken free of interactions that bias it toward the active conformation. This conclusion is supported by the Sos^{Active} trajectory that displays the most severe active-site occlusion (the greatest average number of close contacts with Ras per instantaneous structure) in which the Rem domain never samples a fully active conformation (Figure S7B, right). In this simulation, the Rem domain has overcome

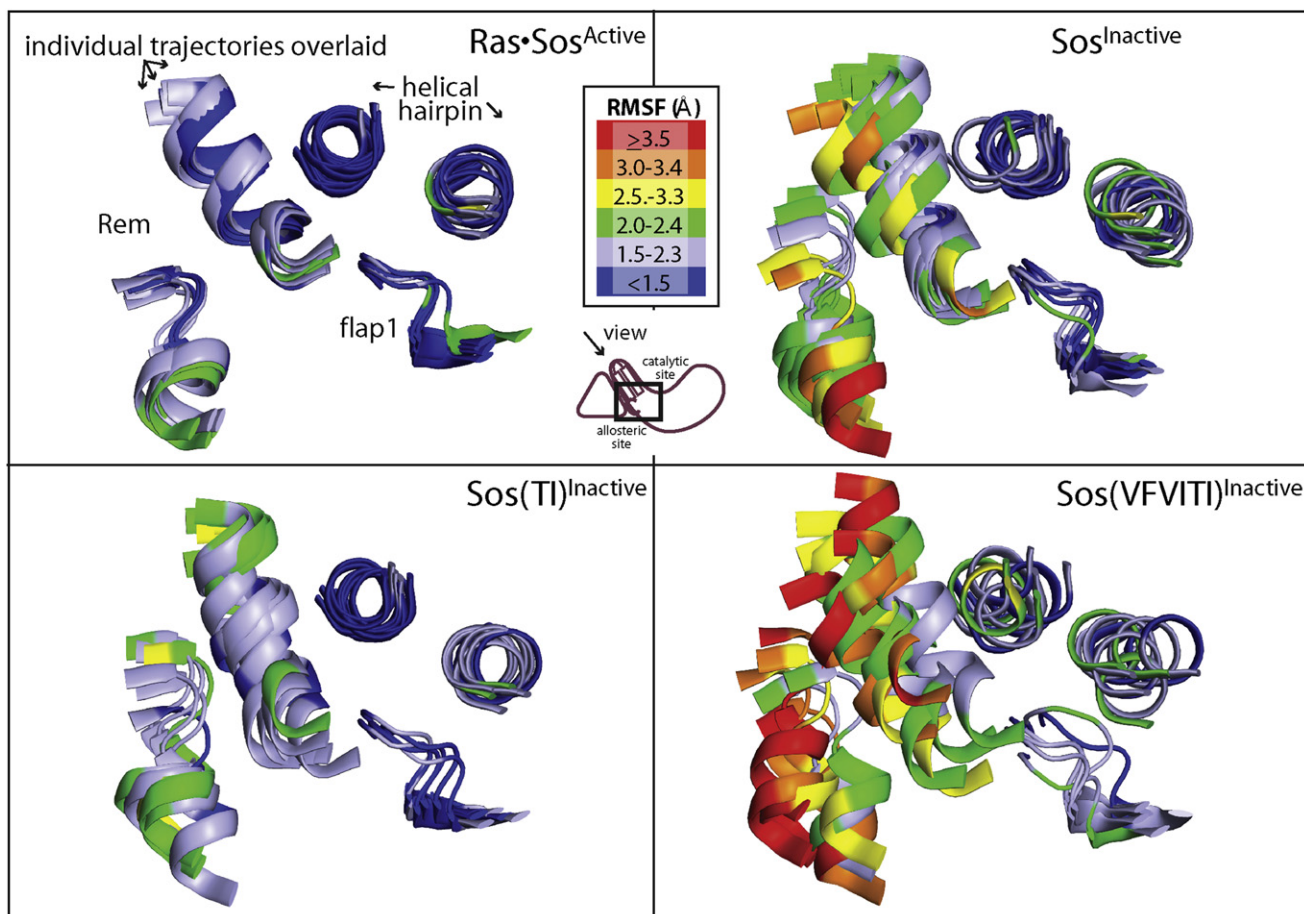


Figure 6. Dynamic Fluctuations and Heterogeneity within Simulations

The rms fluctuation value (related to a crystallographic B factor) of each C_{α} residue is indicated by color. Individual replicates of each simulation are overlaid after alignment on the rigid core of the Cdc25 domain.

some energetic barrier and loses its bias toward the active conformation. Consequently, the helical hairpin fluctuates more often into inactive conformations with an occluded catalytic site. The helical hairpin fluctuates in all the trajectories of $\text{Sos}^{\text{Active}}$ and $\text{Sos}^{\text{Inactive}}$, but only a restricted range of conformations seems to be available to the Rem domain. The correlation of active-site occlusion with the conformational state of the Rem domain pinpoints the Rem domain as the key locking mechanism for the helical hairpin.

Differences in the Trajectories of the Activated Mutants of Sos

As described above, the activated mutant $\text{Sos}(\text{TI})$ is responsive to further stimulation by allosteric Ras binding, whereas further allosteric activation of $\text{Sos}(\text{VFVITI})$ is impaired. We performed simulations of $\text{Sos}(\text{TI})$ and $\text{Sos}(\text{VFVITI})$ starting from the active and inactive crystal structures of wild-type Sos (see *Experimental Procedures*). In all the simulations, the initial steric clash created by inserting the bulkier residues was relieved without any large-scale conformational changes. In simulations of these mutants starting from the inactive structure of Sos ($\text{Sos}(\text{TI})^{\text{Inactive}}$ and $\text{Sos}(\text{VFVITI})^{\text{Inactive}}$, *Table 1*), there is less severe active-site

occlusion than seen in simulations of wild-type $\text{Sos}^{\text{Inactive}}$ (*Figures 4D–4F*).

Although the average position of the helical hairpin is not substantially different in $\text{Sos}(\text{TI})^{\text{Inactive}}$ from that in wild-type $\text{Sos}^{\text{Inactive}}$ (*Figure S5*), the helical hairpin seems to be prevented from sampling conformations in which the active site is completely blocked (*Figure 5C*, surface). Moreover, the trajectories that do show active-site occlusion have fewer close contacts with Ras modeled in the active site (*Figures 4D and 4F*). Although the average position of the Rem domain in the $\text{Sos}(\text{TI})^{\text{Inactive}}$ simulations more closely resembles that of inactive Sos than of active Sos (*Figures 7A–7C*), the β sheet interactions in the Rem domain are extended and have a shifted register, and there are conformational differences in flap1 as well as a helix in the Rem domain that interacts with flap1, the helical hairpin, and allosteric Ras (*Figure 7C*). Furthermore, the Rem domain fluctuates less in the $\text{Sos}(\text{TI})^{\text{Inactive}}$ trajectories than in those of wild-type $\text{Sos}^{\text{Inactive}}$ (*Figure 6C*, colors). We therefore speculate that the Rem domain and helical hairpin in $\text{Sos}(\text{TI})$ are less flexible than in wild-type Sos. The fact that $\text{Sos}(\text{TI})^{\text{Inactive}}$ is not already strongly biased toward the active conformation could explain its sensitivity to further stimulation by allosteric Ras binding.

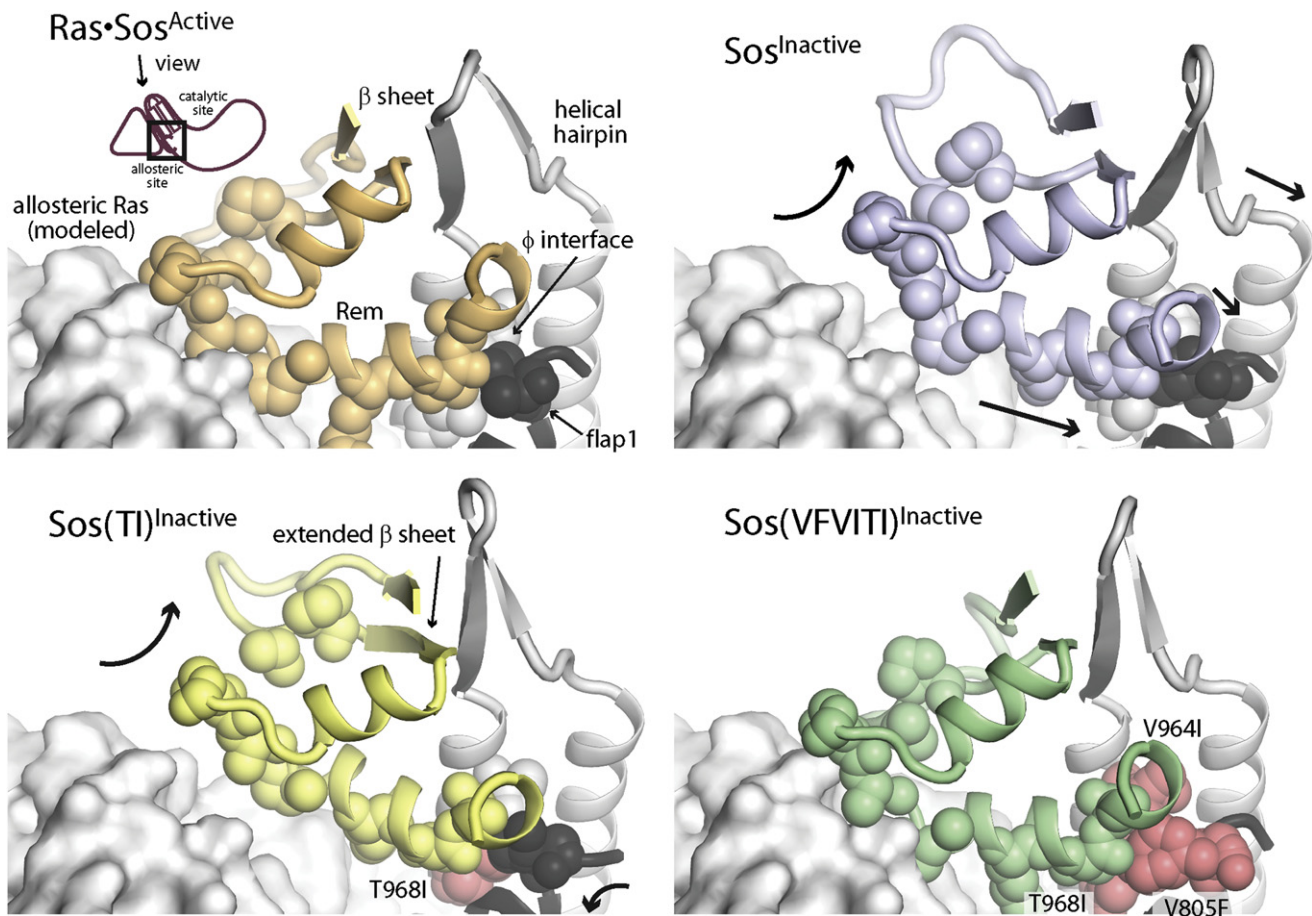


Figure 7. Rem-Domain Position in Wild-Type and Mutant Sos
Average conformation over all simulations. Mutated residues are colored in pink.

Unlike $\text{Sos(TI)}^{\text{Inactive}}$, $\text{Sos(VFVITI)}^{\text{Inactive}}$ is highly flexible. The Rem domains in the $\text{Sos(VFVITI)}^{\text{Inactive}}$ trajectories have high rms fluctuation values (Figure 6D), and $\text{Sos(VFVITI)}^{\text{Inactive}}$ is highly dynamic even in the simulation with the least active-site occlusion (Figure 5D, left, surface). The decrease in active-site occlusion in this mutant seems to arise from increased preference for the active conformation in the absence of allosteric Ras binding. In $\text{Sos(VFVITI)}^{\text{Inactive}}$ the helical hairpin is biased toward the active conformation (Figure S5), and this occurs in conjunction with the Rem domain moving toward the active position (Figure 5D, left panel). This differs from simulations of $\text{Sos}^{\text{Inactive}}$, where the Rem domain does not move into the active position even when the helical hairpin does (Figure 5B, left panel). Moreover, when the average position of the helical hairpin is like that in inactive Sos, as it is in a single $\text{Sos(VFVITI)}^{\text{Inactive}}$ trajectory, the Rem domain is also in the inactive position (Figure 5D, right panel). Intermediate conformations of the Rem domain accompany intermediate conformations of the helical hairpin (Figure S8B), suggesting that the positions of the Rem domain and helical hairpin are better coupled in the Sos(VFVITI) mutant than in wild-type Sos. The average position of the Rem domain over all the simulations of $\text{Sos(VFVITI)}^{\text{Inactive}}$ closely resembles that in $\text{Ras}\cdot\text{Sos}^{\text{Active}}$ (Figures 7A and 7D). Because this mutant no longer requires Ras to achieve the active confor-

mation, its dependence on allosteric activation by Ras could be decreased, explaining the insensitivity of this mutant to further activation by allosteric Ras. It is also possible that the increased flexibility causes a dissipation of the signal generated by allosteric Ras binding, which could result in impaired maximal activity. The idea that flexibility actually impairs the nucleotide exchange reaction is also interesting in light of the observation that RasGRF1 (flexible) is less active than Ras-bound Sos (rigid) even though both are strongly biased toward the active conformation.

We also performed simulations of Sos mutants starting from the active conformation in the absence of Ras ($\text{Sos(TI)}^{\text{Active}}$ and $\text{Sos(VFVITI)}^{\text{Active}}$, Table 1). As wild-type $\text{Sos}^{\text{Active}}$ is already biased toward an active conformation on the nanosecond timescale, any conformational bias created by the mutations is largely masked. Individual simulations of Sos starting from the active conformation remain trapped in the active conformation and generate very few clashes (Figure S5). Two out of seven $\text{Sos}^{\text{Active}}$ trajectories have this restricted profile, whereas three out of six $\text{Sos(TI)}^{\text{Active}}$ simulations have this feature. The triple mutant, however, persists in this state in only one of six simulations (Figure S6). This is consistent with the observation of greater flexibility in the $\text{Sos(VFVITI)}^{\text{Inactive}}$ simulations but not in the $\text{Sos(TI)}^{\text{Inactive}}$ simulations.

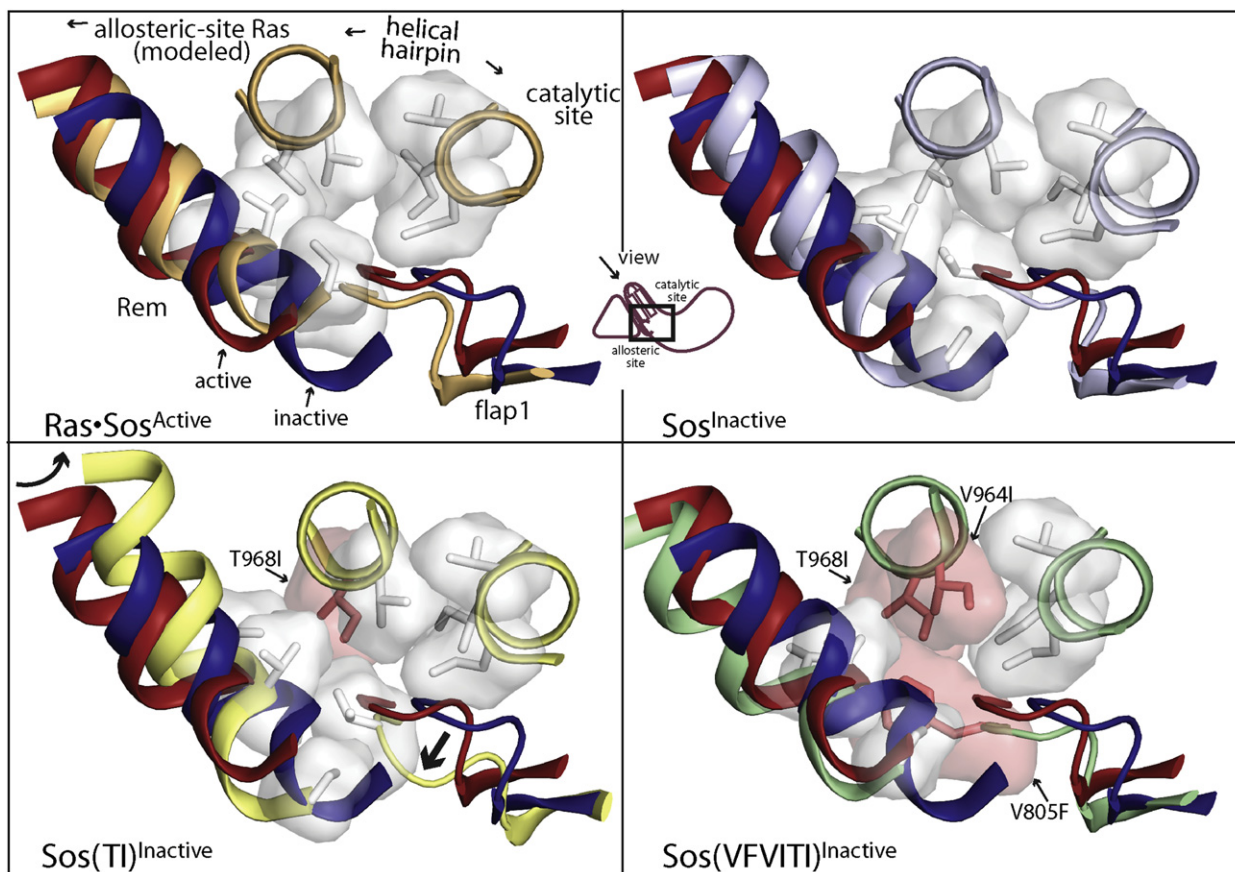


Figure 8. Interface Created by the Rem Domain, Helical Hairpin, and flap1 in the Simulations of Sos

Average conformation over all simulations. Residues participating in the interface of the Rem domain, the helical hairpin, and flap1 are indicated in the surface. Mutated residues are colored in pink. Reference structures for active and inactive Sos are shown in red and blue, respectively.

Comparing the average structure over the simulations of wild-type and mutant Sos, we can speculate about the roles of these mutations in coupling and reorienting the Rem domain and helical hairpin. In the simulations of wild-type Sos, these residues are small, and the interaction of the Rem domain with allosteric Ras is necessary for positioning the Rem domain, and with it the helical hairpin, in the active conformation (Figures 8A and 8B). The bulky isoleucine residue introduced into the helical hairpin (T968I) distorts flap1 and repositions a helix in the Rem domain that forms part of the binding site for allosteric Ras (Figure 8C). The addition of the bulky phenylalanine residue in flap1 and the additional isoleucine residue in the helical hairpin (V805F+V964I) seems to further reorient this helix in the Rem domain, and flap1, into the fully active conformation in the simulations of Sos(VFVITI)^{inactive} (Figure 8D).

DISCUSSION

From our comparison of molecular dynamics trajectories of RasGRF1 and Sos, we suggest that allosteric Ras binding serves two, membrane-independent functions in Sos: to bias Sos toward the active conformation and to decrease the mobility of the helical hairpin, preventing fluctuations that occlude the active site. We believe that this dynamic block on the helical hairpin is

important based on the observation that the catalytic domain of RasGRF1 populates a set of conformations that is biased toward an active position, but is nonetheless a much less efficient exchange factor than activated Sos.

Whereas it seems clear from the simulations that Sos(TI) and Sos(VFVITI) have higher basal activities because they are more receptive to Ras binding at the active site, the manner in which they achieve this is surprising. The Rem domain of Sos(VFVITI) is biased toward the active conformation, but at the expense of high flexibility. Sos(TI), however, samples highly clashing conformations less often, probably because of decreased overall flexibility. The observation from molecular dynamics that the Rem domain of Sos(VFVITI), but not of Sos(TI), is biased toward the active conformation is consistent with the measured affinities of their allosteric sites for Ras. Sos(VFVITI) binds allosteric Ras with higher affinity than does wild-type Sos; increased population of an active-like conformation could lessen the entropic penalty of binding. The affinity of Sos(TI) for allosteric Ras remains unchanged, and in the Sos(TI)^{inactive} trajectories the Rem domain does not shift toward the active conformation.

We had previously proposed that the bulky residues that pack the helical hairpin/flap1 interface of RasGRF1 contribute to its ability to maintain an active conformation by holding open the active conformation (Freedman et al., 2006). Based on our

molecular dynamics simulations, we now refine our analysis of the role of these residues. It seems that the helical hairpin of Sos is intrinsically flexible and samples a variety of conformations along with the Rem domain. We see in our simulations that the active conformation of the helical hairpin is not incompatible with the inactive conformation of the Rem domain. Conformations in which the Rem domain appears to be in an inactive position but the helical hairpin is still pivoted outward have also been observed in a crystal structure. In one of two molecules in the crystallographic asymmetric unit of Sos^{DH-PH-Cdc25}, the hydrophobic interface between the helical hairpin and the Rem domain is also broken, suggesting a mechanism for how the position of the helical hairpin may be uncoupled from the Rem domain (Sondermann et al., 2004). However, we never observe the helical hairpin to be in an inactive position if the Rem domain has adopted an active position.

A large component of the regulatory apparatus of Sos relies on the intrinsic inactivity of the catalytic Cdc25 domain. Unlike other regulators of the Ras pathway that have been linked to forms of Noonan syndrome, Sos does not cause Noonan syndrome-associated cancers (Roberts et al., 2007; Swanson et al., 2008; Tartaglia et al., 2007). This could be because the autoregulation of Sos has many checkpoint steps, including release of the histone domain, release of the DH domain, clustering of Ras, and production of Ras•GTP to bind to the allosteric site (Gur-easko et al., 2008; Margarit et al., 2003). In addition, Sos is regulated by phosphorylation, adaptor binding, and recruitment to activated receptors. If the catalytic site of Sos were active in the absence of allosteric activation, this regulation could be bypassed, leading to a much more severe hyperactivation of Ras. The intrinsic inactivity of its catalytic domain may explain why Sos has yet to be implicated in human cancers. The helical hairpin of the Rap exchange factor Epac2 undergoes analogous movements to Sos in the switch from active to inactive, but this motion is subtler than the conformational change observed in Sos, and the activator binding domain in this protein directly occludes the active site (Rehmann et al., 2006, 2008). Unlike Sos and Epac2, the helical hairpin of RasGRF1 does not seem to collapse inward to block the catalytic site. The levels of RasGRF1 in cells are tightly regulated by cell- and environment-specific expression and by proteolysis (Baouz et al., 1997; Cen et al., 1992; Coccetti et al., 1995; Leaner et al., 2005; Martegani et al., 1992). Thus, it is possible that RasGRF1 may not require the strict control of activity that drove the evolution of a fail-safe mechanism in Sos.

EXPERIMENTAL PROCEDURES

Protein Purification

We purified Sos^{cat} (human Sos1, residues 566–1049 in pPROEX vector), RasGRF1^{Cdc25} (mouse RasGRF1, residues 1028–1262 in pGEX-6P-3 vector), and Ras (human H-Ras, residues 1–166 in pPROEX vector) as described previously (Freedman et al., 2006). Briefly, we harvested protein from BL21 DE3* cells (Novagen) after induction with 0.1 mM isopropyl β-D-1-thiogalactopyranoside at 18°C for ~16 hr. We performed affinity chromatography (HiTrap for Sos and Ras, GStrap for RasGRF1; Amersham) followed by ion-exchange chromatography (HiTrap Q for Sos and Ras, HiTrap S for RasGRF1; Amersham). We then transferred protein into the final buffer (200 mM NaCl and 25 mM Tris [pH 8.0]) by gel filtration (Superdex 200; Amersham). SDS-PAGE and mass spectrometry confirmed protein homogeneity. We measured protein concentration (30 mg/ml) by absorbance at 280 nm (Gasteiger et al., 2005),

which agreed with values obtained in guanidinium chloride (Gill and von Hippel, 1989) and with results of bicinchoninic acid (BCA) colorimetric assays (Sigma). Protein aliquots were frozen in liquid nitrogen and stored at –80°C. The concentration of nucleotide-bound Ras was only measured by the BCA assay. We performed site-directed mutagenesis on Sos with the QuikChange system (Invitrogen) and verified the clones by sequencing. We attempted to make the reciprocal RasGRF1 mutants, but even conservative mutants of RasGRF1 were aggregated or insoluble.

Measurement of Ras-Specific Nucleotide Exchange Activity and Affinity of Ras for the Allosteric Site of Sos

We measured the decrease in fluorescence as a fluorescent GDP analog was released from Ras to determine the relative activities of RasGRF1 and Sos (Lenzen et al., 1995). Nucleotide exchange reactions were initiated by rapid 1:1 mixing of 2 μM Sos (in a starting mixture of 400 μM GDP, 40 mM HEPES [pH 7.5], 10 mM MgCl₂, and 1 mM DTT) with 0.2 μM Ras preloaded with 3'-O-N-methyl-anthraniloyl-2'-deoxy-guanosine-5'-diphosphate (Ras•mant-dGDP; Jena Bioscience; Guo et al., 2005) in 40 mM HEPES [pH 7.5], 10 mM MgCl₂, and 1 mM DTT on a stopped-flow apparatus (Applied Photophysics RX2000) linked to a Jobin Yvon Horiba Fluoromax-3 fluorimeter. After this 2-fold dilution, the final concentration of Sos was 1 μM and the final concentration of substrate Ras was 0.1 μM. We premixed Ras^{Y64A}•GMPPNP with Sos in some reactions to measure allosteric activation of Sos by Ras. To prevent precipitation of RasGRF1 (Freedman et al., 2006; Lenzen et al., 1995) and allow comparison between RasGRF1 and Sos, the samples, the stopped-flow apparatus, and the cuvette were chilled to 15°C before mixing. The progress of each 300 μl reaction was monitored by fluorescence intensity at 430 nm upon excitation at 370 nm. Excitation slits were fixed at 5 nm, and data were recorded every 0.5 s after integration over 0.05 s. Emission slits were set to maximize signal without exceeding the linear range of the instrument, generally between 15 and 25 nm. Whenever possible, reactions were carried out for 20 times the half-life of the nucleotide exchange reaction. Data were obtained by averaging three consecutive runs with the same sample, and each reaction was performed in triplicate with independent protein samples.

We used Prism 5.0 (Graphpad) to fit the decay curves to a double exponential function ($Y = A_0 + A_1 \cdot e^{-k_1 \cdot t} + A_2 \cdot e^{-k_2 \cdot t}$), where the higher-amplitude phase was the nucleotide exchange rate and the invariant, lower-amplitude phase was attributed to photobleaching. After fitting, we normalized the raw data independently for each reaction with the formula $Y_{\text{normalized}} = (Y_{\text{raw}} - A_0) / (\text{Max} - A_0)$, where A_0 represents the offset value from the exponential fit and Max is the initial, maximum fluorescence of the sample.

To measure the affinity of Ras for the allosteric site of Sos, the rates of nucleotide release versus concentration/ratio of added Ras^{Y64A}, a mutant of Ras that binds only to the allosteric site, were fit to a hyperbolic binding model $y = y_0 + (B_{\text{max}} \cdot x) / (K_d + x)$, where B_{max} is the maximum activity when the allosteric site of Sos is saturated with Ras^{Y64A}. The offset, y_0 , was used to account for differences in the basal activity of each mutant in the absence of added Ras^{Y64A}.

Molecular Dynamics Simulations

Individual molecular dynamics simulations are summarized in Table 1. Two loops that are disordered in the crystal structure of Sos were built using O (Kleywegt and Jones, 1996). To generate the mutants of Sos for simulation, we used PyMOL (DeLano, 2002) to model the substitution. Rotamers of the substituted residues were selected based on their appearance in the structure of RasGRF1 (Freedman et al., 2006). Each starting structure, with crystallographic water molecules removed, was placed in a rectangular water box that extended 10 Å beyond the limits of the protein, and Na⁺ and Cl⁻ ions corresponding to a concentration of ~150 mM. If necessary, extra chloride ions were added to offset the intrinsic charge of the protein. All simulations were performed with the TIP3P explicit water model (Jorgensen et al., 1983). These steps were performed using the LEAP module of AMBER, version 7, with the parm96 force field (Cornell et al., 1995; Pearlman et al., 1995). The charge-charge conflict presented by the proximity of Glu-873 and Asp-792 was removed by protonating Asp-792 (the significance of this interaction, observed in the crystal structures, is not well understood). The ε nitrogen on His-827 in this cluster of residues was protonated to allow interactions with Glu-792 (a proton on the δ nitrogen of this residue would have no interactions); all other histidine residues were left in the default state of protonation selected

by AMBER. After equilibration with positional restraints for the first 50 ps, random velocities were assigned to the atoms (Young et al., 2001). Each starting condition was used to generate 6–8 trajectories, initiated with different random velocities. Each simulation was carried out for at least 7 ns at a constant pressure of 1 atm and a constant temperature of 298K.

The first nanosecond of each simulation was omitted from our analysis to eliminate the effects of initial relaxation. We analyzed the simulations with CHARMM (Brooks et al., 1983) and PyMOL (DeLano, 2002). We used CHARMM to calculate average structures from every 10 ps of simulation to approximate instantaneous structures in our analysis. We also used CHARMM to calculate the average structure for each simulation. For this and subsequent analysis, we aligned all instantaneous structures on the rigid core of the Cdc25 domain (residues 1029–1041, 1087–1114, and 1134–1147 for RasGRF1 or residues 782–794, 839–867, and 888–899 for Sos). CHARMM was also used to calculate rms fluctuation ($\langle \Delta r_i^2 \rangle^{0.5}$), which is related to the crystallographic B value by the formula $\langle \Delta r_i^2 \rangle = 3B_i/8\pi^2$. We calculated rmsd's between the structures from the trajectories and the starting structures with PyMOL, using a python script to iteratively perform the "rms_cur" command and print the rmsd values for each 10 ns of each trajectory. The residues in the Rem domain that interact with allosteric Ras (residues 683–695 and 615–621) and the helical hairpin (residues 929–943 and 958–976 for Sos, residues 1178–1193 and 1204–1222 for RasGRF1) were compared independently.

To calculate the average structure over multiple simulations, we used a python script developed in the McCommon laboratory (http://mccommon.ucsd.edu/~cmura/PyMOL/pymol_mainFrame.html). The average structure does not correspond to a structure actually sampled during the simulations, and has meaningless stereochemistry. For Figures 3, 7, and 8 and Figure S5, we used the average structure to select instantaneous structures from the trajectory that have the closest correspondence to the helical hairpin and to the Rem domain. We confirmed these choices by visual inspection.

A python script in PyMOL was used to list the number of steric clashes between the backbone atoms of the helical hairpin (residues 1178–1193 of RasGRF1 or residues 929–976 of Sos) that lie less than 2.2 Å away from a position occupied by Ras in the active site of Sos^{cat} in the crystal structure (Protein Data Bank [PDB] ID code 1NVV; Margarit et al., 2003). For this calculation, we used residues in Ras that surround the anchoring residue Y64. We avoided using residues that belong to the extended region of switch 2 that is opened by binding to the helical hairpin, because it is not clear whether this is the conformation from which Ras would be recognized by Sos, and interactions in the structure of active Sos are very close. In short, we used residues 15–26 and 56–74 of Ras for our calculation. The cutoff for our definition of a steric clash, 2.2 Å, was chosen based on the estimated van der Waals radii of the backbone atoms nitrogen, oxygen, and carbon. These have a range of van der Waals radii from 1.38 to 1.55 (for carbon and oxygen, respectively; Martz and Sayle, 2000). Steric clash has been defined as occurring when the distance between two backbone atoms is smaller than 70% of the sum of the van der Waals radii (Fernandez-Fuentes et al., 2006a, 2006b). For two oxygen atoms, this puts the cutoff at 2.2 Å.

SUPPLEMENTAL DATA

Supplemental Data include eight figures and can be found with this article online at [http://www.cell.com/structure/supplemental/S0969-2126\(08\)00428-0](http://www.cell.com/structure/supplemental/S0969-2126(08)00428-0).

ACKNOWLEDGMENTS

We thank Doug Lowy for RasGRF1 cDNA, Jodi Gureasko, Nick Levinson, and Xuewu Zhang for interesting discussions, and David King for mass spectrometry. We thank Susan Marqusee and Dafna Bar-Sagi for guidance and discussions. H.S. was supported by the Leukemia and Lymphoma Society. G.D.F. is supported by the NSFGRFP, and T.K. by the Sloan Foundation. J.K. is supported by the NCI (R01 CA096504-02).

Received: July 26, 2008

Revised: October 30, 2008

Accepted: November 3, 2008

Published: January 13, 2009

REFERENCES

- Baouz, S., Jacquet, E., Bernardi, A., and Parmeggiani, A. (1997). The N-terminal moiety of CDC25(Mm), a GDP/GTP exchange factor of Ras proteins, controls the activity of the catalytic domain. Modulation by calmodulin and calpain. *J. Biol. Chem.* *272*, 6671–6676.
- Boriack-Sjodin, P.A., Margarit, S.M., Bar-Sagi, D., and Kuriyan, J. (1998). The structural basis of the activation of Ras by Sos. *Nature* *394*, 337–343.
- Brooks, B.R., Bruccoleri, R.E., Olafson, B.D., States, D.J., Swaminathan, S., and Karplus, M. (1983). CHARMM: a program for macromolecular energy, minimization, and dynamics calculations. *J. Comput. Chem.* *4*, 187–217.
- Cen, H., Papageorge, A.G., Zippel, R., Lowy, D.R., and Zhang, K. (1992). Isolation of multiple mouse cDNAs with coding homology to *Saccharomyces cerevisiae* CDC25: identification of a region related to Bcr, Vav, Dbl and CDC24. *EMBO J.* *11*, 4007–4015.
- Cocchetti, P., Mauri, I., Alberghina, L., Martegani, E., and Parmeggiani, A. (1995). The minimal active domain of the mouse ras exchange factor CDC25Mm. *Biochem. Biophys. Res. Commun.* *206*, 253–259.
- Coleman, M.L., Marshall, C.J., and Olson, M.F. (2004). RAS and RHO GTPases in G1-phase cell-cycle regulation. *Nat. Rev. Mol. Cell Biol.* *5*, 355–366.
- Cornell, W.D., Cieplak, P., Bayly, C.I., Gould, I.R., Merz, K.M., Ferguson, D.M., Spellmeyer, D.C., Fox, T., Caldwell, J.W., and Kollman, P.A. (1995). A second generation force field for the simulation of proteins, nucleic acids, and organic molecules. *J. Am. Chem. Soc.* *117*, 5179–5197.
- DeLano, W.L. (2002). The PyMOL Molecular Graphics System (<http://www.pymol.org>).
- Dodson, G.G., Lane, D.P., and Verma, C.S. (2008). Molecular simulations of protein dynamics: new windows on mechanisms in biology. *EMBO Rep.* *9*, 144–150.
- Egan, S.E., Giddings, B.W., Brooks, M.W., Buday, L., Sizeland, A.M., and Weinberg, R.A. (1993). Association of Sos Ras exchange protein with Grb2 is implicated in tyrosine kinase signal transduction and transformation. *Nature* *363*, 45–51.
- Fernandez-Fuentes, N., Oliva, B., and Fiser, A. (2006a). A supersecondary structure library and search algorithm for modeling loops in protein structures. *Nucleic Acids Res.* *34*, 2085–2097.
- Fernandez-Fuentes, N., Zhai, J., and Fiser, A. (2006b). ArchPRED: a template based loop structure prediction server. *Nucleic Acids Res.* *34*, W173–W176.
- Freedman, T.S., Sondermann, H., Friedland, G.D., Kortemme, T., Bar-Sagi, D., Marqusee, S., and Kuriyan, J. (2006). A Ras-induced conformational switch in the Ras activator Son of sevenless. *Proc. Natl. Acad. Sci. USA* *103*, 16692–16697.
- Gasteiger, E.H.C., Hoogland, C., Gattiker, A., Duvaud, S., Wilkins, M.R., Appel, R.D., and Bairoch, A. (2005). Protein identification and analysis tools on the ExPASy server. In *The Proteomics Protocols Handbook*, J.M. Walker, ed. (Totowa, NJ: Humana Press), pp. 571–607.
- Gill, S.C., and von Hippel, P.H. (1989). Calculation of protein extinction coefficients from amino-acid sequence data. *Anal. Biochem.* *182*, 319–326.
- Guo, Z., Ahmadian, M.R., and Goody, R.S. (2005). Guanine nucleotide exchange factors operate by a simple allosteric competitive mechanism. *Biochemistry* *44*, 15423–15429.
- Gureasko, J., Galush, W.J., Boykevich, S., Sondermann, H., Bar-Sagi, D., Groves, J.T., and Kuriyan, J. (2008). Membrane-dependent signal integration by the Ras activator Son of sevenless. *Nat. Struct. Mol. Biol.* *15*, 452–461.
- Hall, B.E., Yang, S.S., Boriack-Sjodin, P.A., Kuriyan, J., and Bar-Sagi, D. (2001). Structure-based mutagenesis reveals distinct functions for Ras switch 1 and switch 2 in Sos-catalyzed guanine nucleotide exchange. *J. Biol. Chem.* *276*, 27629–27637.
- Hanahan, D., and Weinberg, R.A. (2000). The hallmarks of cancer. *Cell* *100*, 57–70.
- Herrmann, C., and Nassar, N. (1996). Ras and its effectors. *Prog. Biophys. Mol. Biol.* *66*, 1–41.

- Jorgensen, W.L., Chandrasekhar, J., Madura, J.D., Impey, R.W., and Klein, M.L. (1983). Comparison of simple potential functions for simulating liquid water. *J. Chem. Phys.* **79**, 926–935.
- Karplus, M., and Kuriyan, J. (2005). Molecular dynamics and protein function. *Proc. Natl. Acad. Sci. USA* **102**, 6679–6685.
- Kleywegt, G.J., and Jones, T.A. (1996). Efficient rebuilding of protein structures. *Acta Crystallogr. D Biol. Crystallogr.* **52**, 829–832.
- Leaner, V.D., Donninger, H., Ellis, C.A., Clark, G.J., and Birrer, M.J. (2005). p75-Ras-GRF1 is a c-Jun/AP-1 target protein: its up regulation results in increased Ras activity and is necessary for c-Jun-induced nonadherent growth of Rat1a cells. *Mol. Cell. Biol.* **25**, 3324–3337.
- Lenzen, C., Cool, R.H., and Wittinghofer, A. (1995). Analysis of intrinsic and CDC25-stimulated guanine nucleotide exchange of p21ras-nucleotide complexes by fluorescence measurements. *Methods Enzymol.* **255**, 95–109.
- Lenzen, C., Cool, R.H., Prinz, H., Kuhlmann, J., and Wittinghofer, A. (1998). Kinetic analysis by fluorescence of the interaction between Ras and the catalytic domain of the guanine nucleotide exchange factor Cdc25Mm. *Biochemistry* **37**, 7420–7430.
- Margarit, S.M., Sondermann, H., Hall, B.E., Nagar, B., Hoelz, A., Pirruccello, M., Bar-Sagi, D., and Kuriyan, J. (2003). Structural evidence for feedback activation by Ras•GTP of the Ras-specific nucleotide exchange factor SOS. *Cell* **112**, 685–695.
- Martegani, E., Vanoni, M., Zippel, R., Coccetti, P., Brambilla, R., Ferrari, C., Sturani, E., and Alberghina, L. (1992). Cloning by functional complementation of a mouse cDNA encoding a homologue of CDC25, a *Saccharomyces cerevisiae* RAS activator. *EMBO J.* **11**, 2151–2157.
- Martz, E., and Sayle, R. (2000). What Are the Values Used by RasMol and Chime for van der Waals Radii in the Spacefill Rendering? (<http://www.umass.edu/microbio/rasmol/rasbonds.htm>).
- Pearlman, D.A., Case, D.A., Caldwell, J.W., Ross, W.S., Cheatham, T.E., Debolt, S., Ferguson, D., Seibel, G., and Kollman, P. (1995). AMBER, a package of computer-programs for applying molecular mechanics, normal-mode analysis, molecular-dynamics and free-energy calculations to simulate the structural and energetic properties of molecules. *Comput. Phys. Commun.* **91**, 1–41.
- Rehmann, H., Das, J., Knipscheer, P., Wittinghofer, A., and Bos, J.L. (2006). Structure of the cyclic-AMP-responsive exchange factor Epac2 in its auto-inhibited state. *Nature* **439**, 625–628.
- Rehmann, H., Arias-Palomo, E., Hadders, M.A., Schwede, F., Llorca, O., and Bos, J.L. (2008). Structure of Epac2 in complex with a cyclic AMP analogue and RAP1B. *Nature* **455**, 124–127.
- Roberts, A.E., Araki, T., Swanson, K.D., Montgomery, K.T., Schiripo, T.A., Joshi, V.A., Li, L., Yassin, Y., Tamburino, A.M., Neel, B.G., and Kucherlapati, R.S. (2007). Germline gain-of-function mutations in SOS1 cause Noonan syndrome. *Nat. Genet.* **39**, 70–74.
- Schubbert, S., Shannon, K., and Bollag, G. (2007). Hyperactive Ras in developmental disorders and cancer. *Nat. Rev. Cancer* **7**, 295–308.
- Sondermann, H., Soisson, S.M., Boykevich, S., Yang, S.S., Bar-Sagi, D., and Kuriyan, J. (2004). Structural analysis of autoinhibition in the Ras activator Son of sevenless. *Cell* **119**, 393–405.
- Sondermann, H., Nagar, B., Bar-Sagi, D., and Kuriyan, J. (2005). Computational docking and solution X-ray scattering predict a membrane-interacting role for the histone domain of the Ras activator son of sevenless. *Proc. Natl. Acad. Sci. USA* **102**, 16632–16637.
- Swanson, K.D., Winter, J.M., Reis, M., Bentires-Alj, M., Greulich, H., Grewal, R., Hruban, R.H., Yeo, C.J., Yassin, Y., Iartchouk, O., et al. (2008). SOS1 mutations are rare in human malignancies: implications for Noonan syndrome patients. *Genes Chromosomes Cancer* **47**, 253–259.
- Tartaglia, M., Pennacchio, L.A., Zhao, C., Yadav, K.K., Fodale, V., Sarkozy, A., Pandit, B., Oishi, K., Martinelli, S., Schackwitz, W., et al. (2007). Gain-of-function SOS1 mutations cause a distinctive form of Noonan syndrome. *Nat. Genet.* **39**, 75–79.
- Vetter, I.R., and Wittinghofer, A. (2001). The guanine nucleotide-binding switch in three dimensions. *Science* **294**, 1299–1304.
- Young, M.A., Gonfloni, S., Superti-Furga, G., Roux, B., and Kuriyan, J. (2001). Dynamic coupling between the SH2 and SH3 domains of c-Src and Hck underlies their inactivation by C-terminal tyrosine phosphorylation. *Cell* **105**, 115–126.

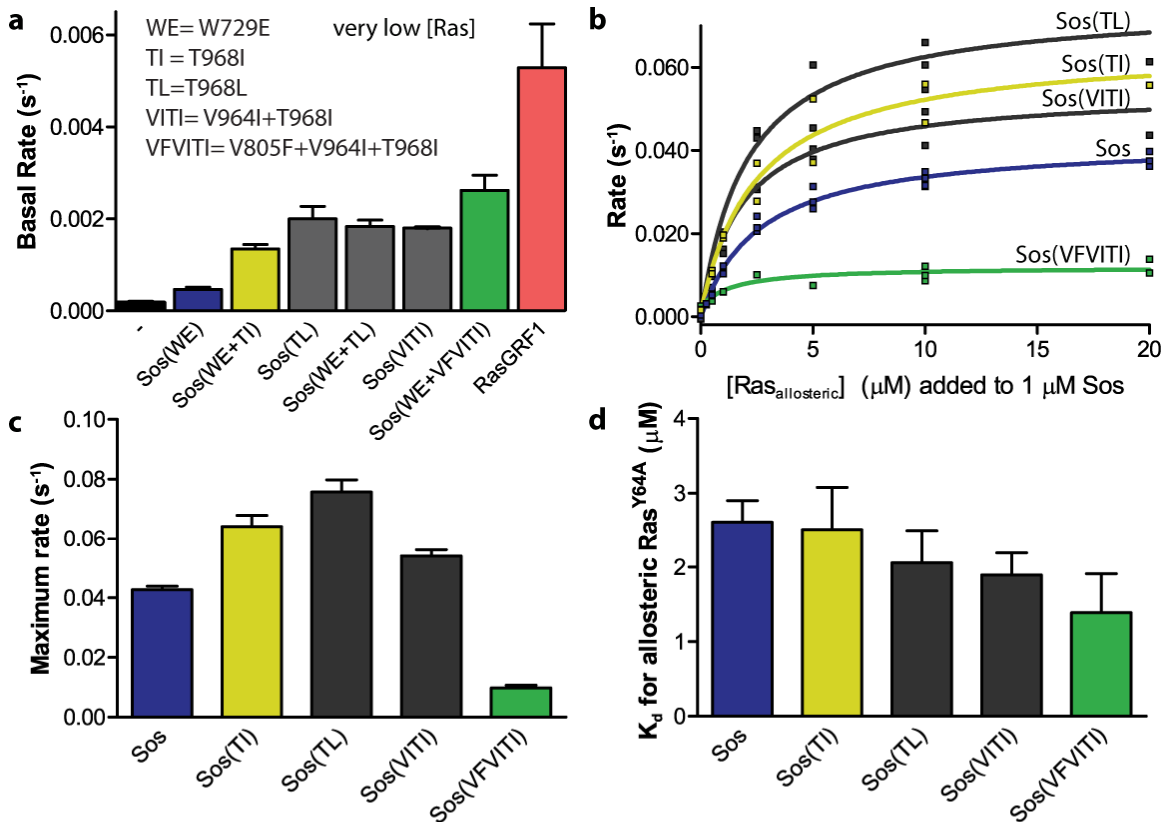
Supplemental Data

Differences in Flexibility Underlie Functional

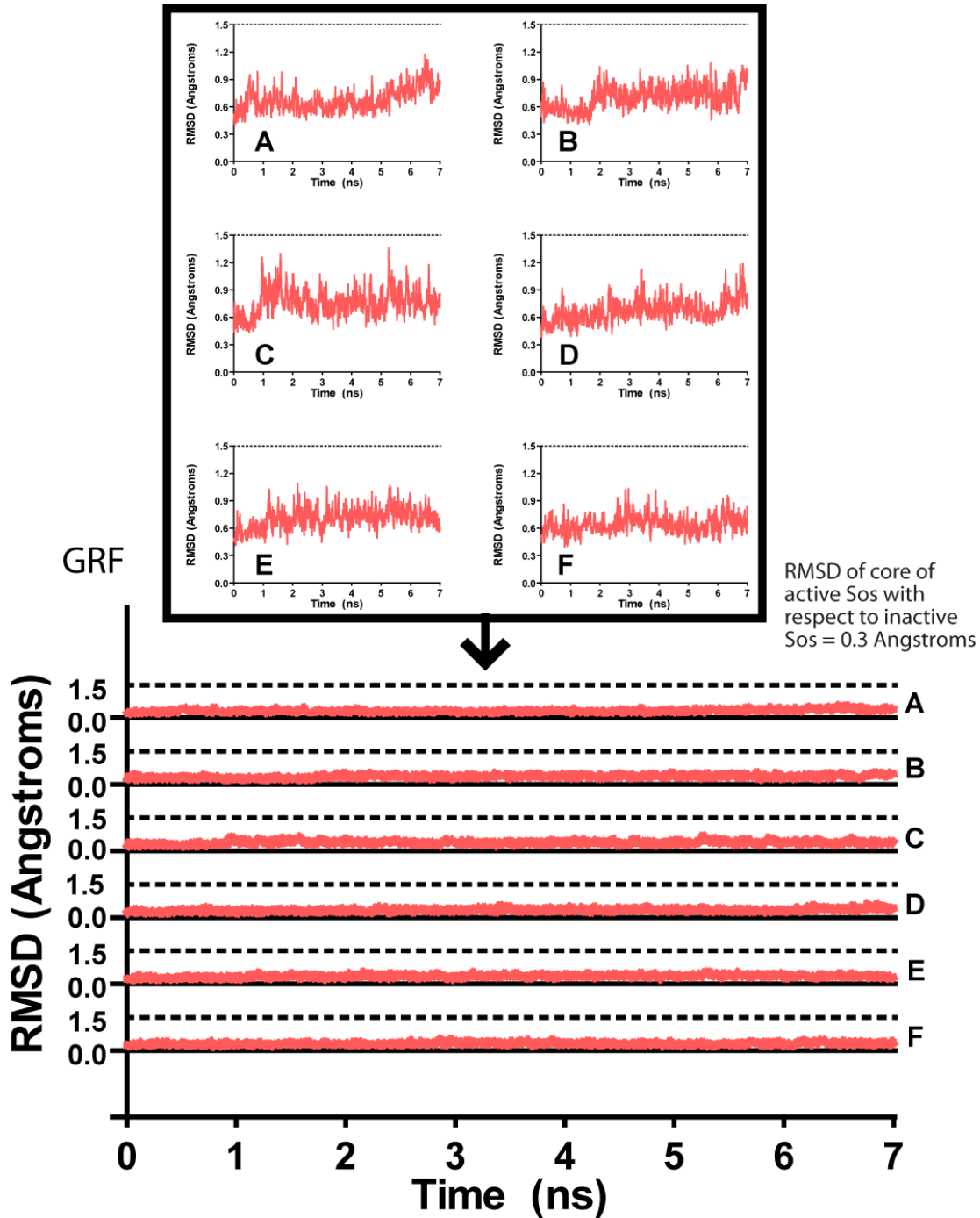
Differences in the Ras Activators Son of Sevenless

and Ras Guanine Nucleotide Releasing Factor 1

Tanya S. Freedman, Holger Sondermann, Olga Kuchment, Gregory D. Friedland, Tanja Kortemme, and John Kuriyan

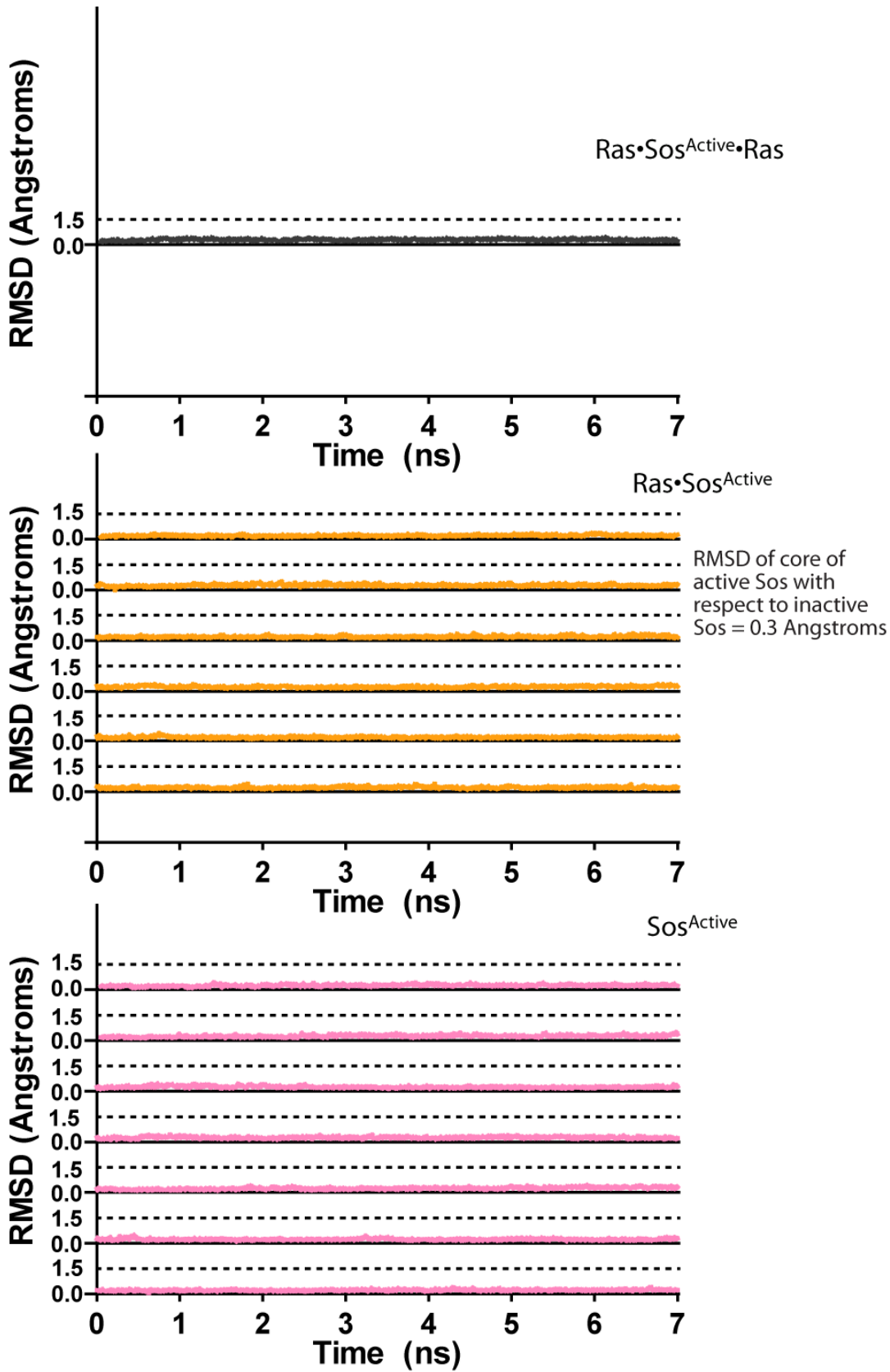


Supplementary Fig. 1. Activity and response to allosteric Ras of activated Sos mutants. **(a)** Additional mutations in the helical hairpin and flap1 result in increased basal activity of Sos. Activity is unaffected by introduction of the Rem-domain mutation W729E, which blocks allosteric Ras binding. Errors represent the mean \pm the standard deviation of the fit rates for at least three separate experiments. **(b)** By adding Ras^{Y64A} to the reactions, we determined the sensitivity of the mutants to further stimulation by allosteric Ras binding and fit the binding curves to determine **(c)** the maximum stimulated rate upon saturation of the allosteric site **(d)** and the affinity of Ras for the allosteric site.



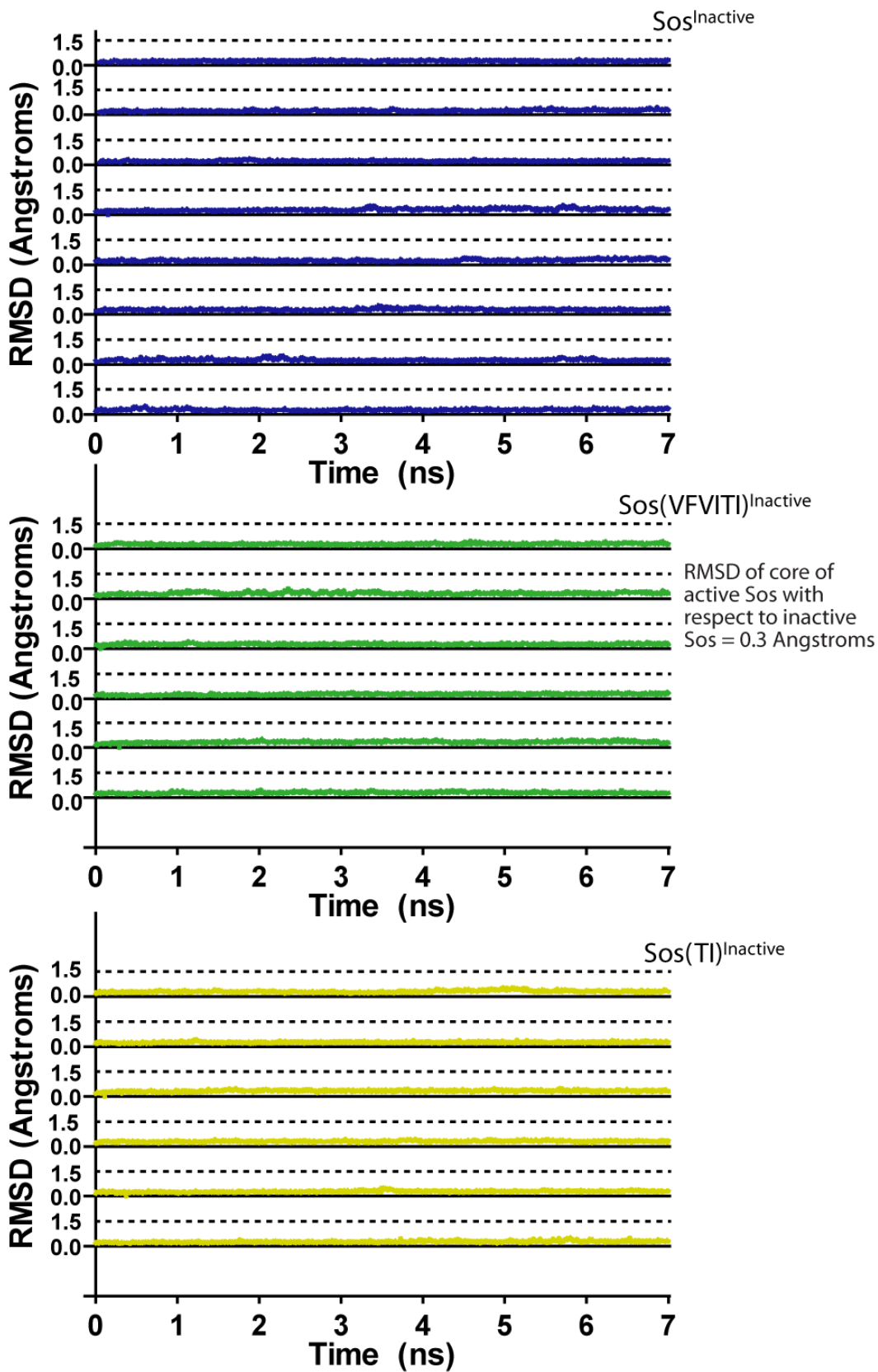
Supplementary Fig. 2. RMSD values of C_{α} residues in the core of the Cdc25 domain with respect to the starting structure. Replicates of the same simulation are shifted vertically by increments of 6 Å to facilitate visualization. After alignment, RMSD values for every 10 ps of each simulation were calculated with respect to equivalent residues from the crystal structure of RasGRF1 (GRF), active Sos (Ras•Sos^{Active}•Ras, Ras•Sos^{Active}, Sos^{Active}, Sos(TI)^{Active}, and Sos(VFVITI)^{Active}), or inactive Sos (Sos^{Inactive}, Sos(TI)^{Inactive}, and Sos(VFVITI)^{Inactive}).

Continued on next page



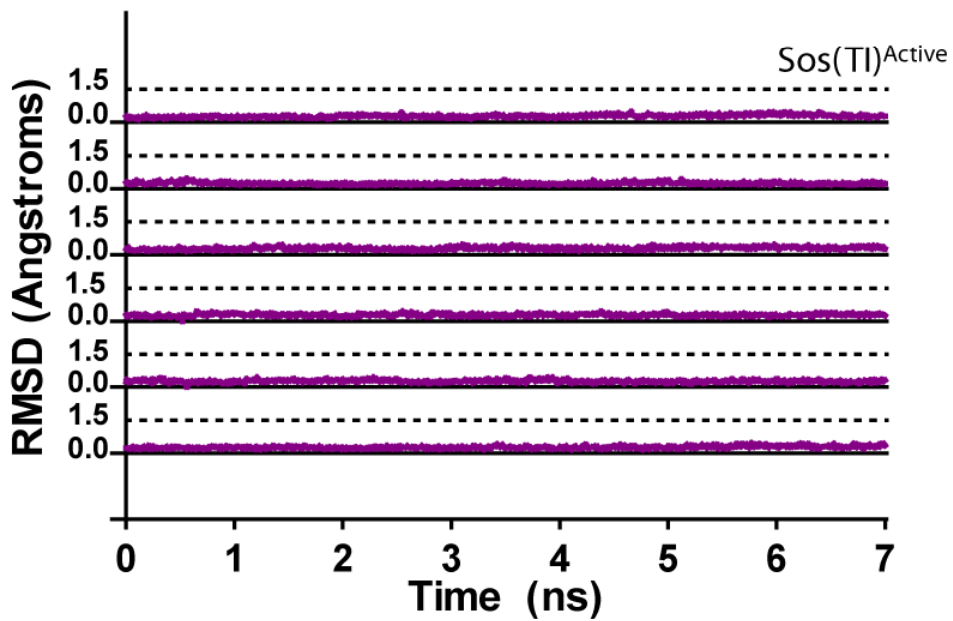
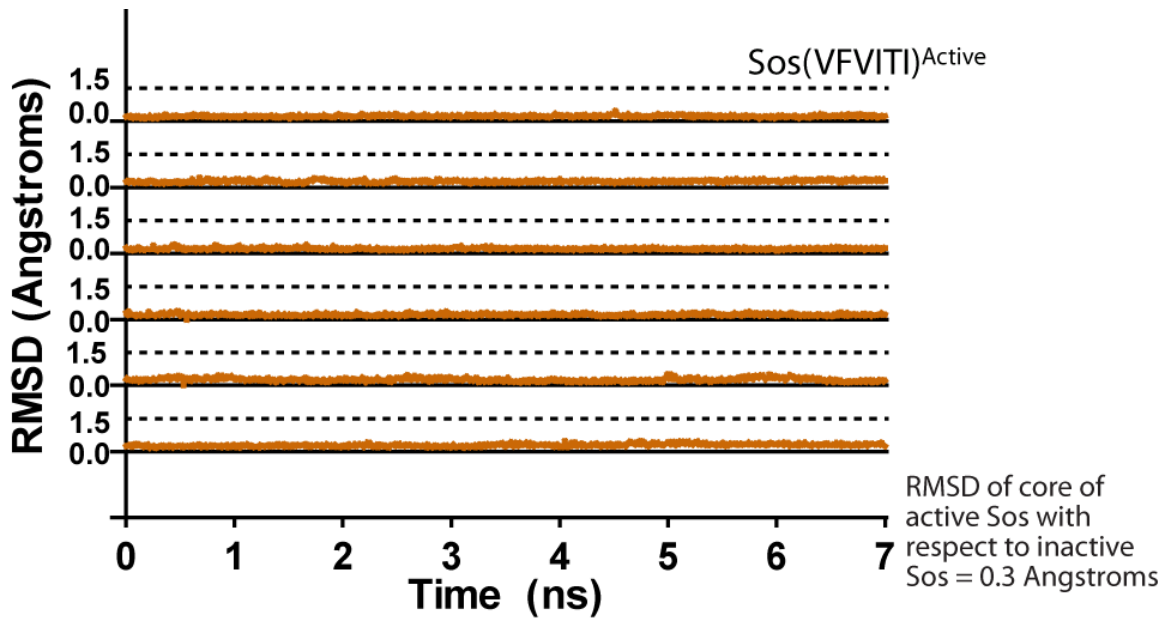
Supplementary Fig. 2. Ctd.

Continued on next page

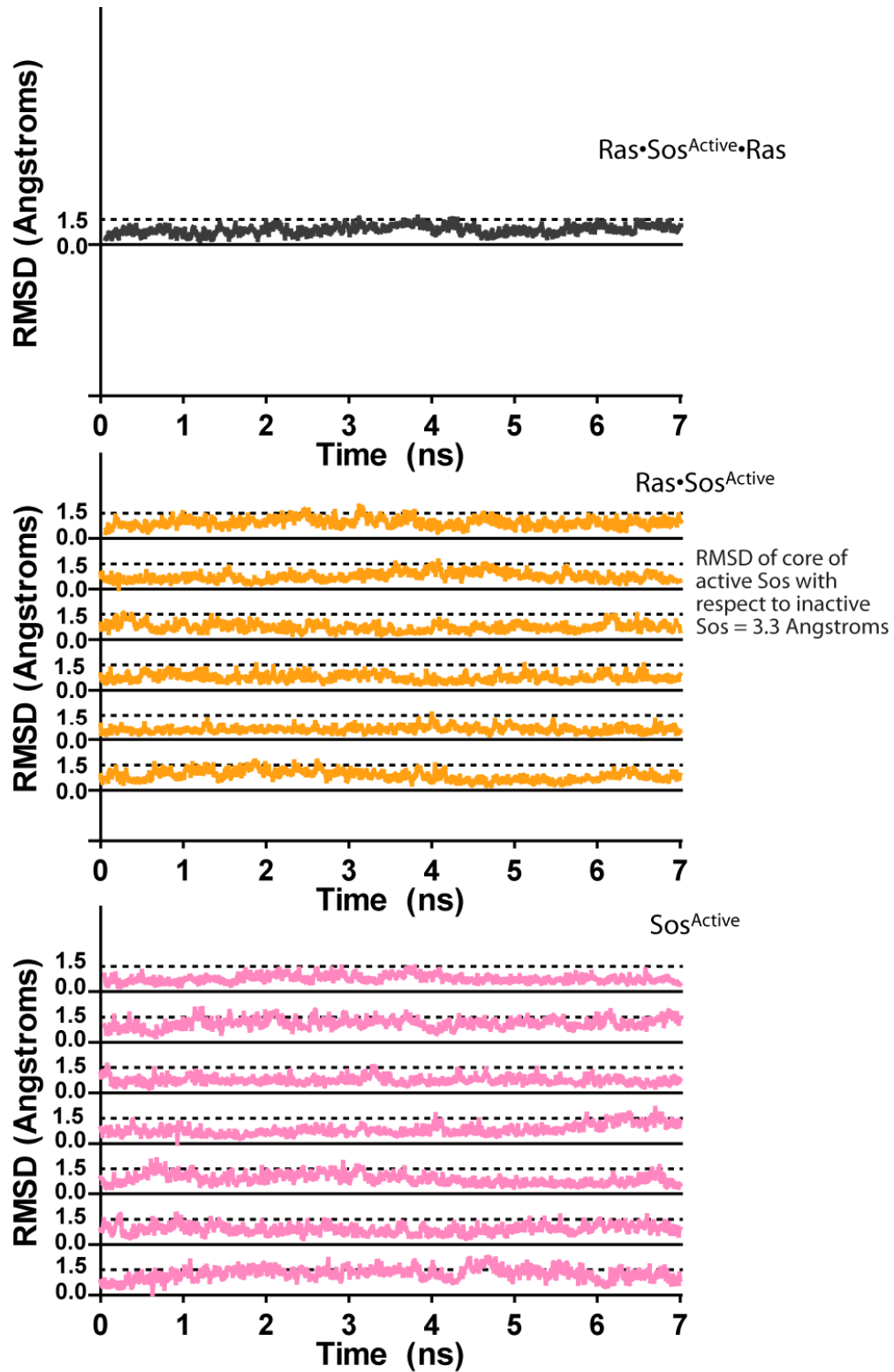


Supplementary Fig. 2. Ctd.

Continued on next page

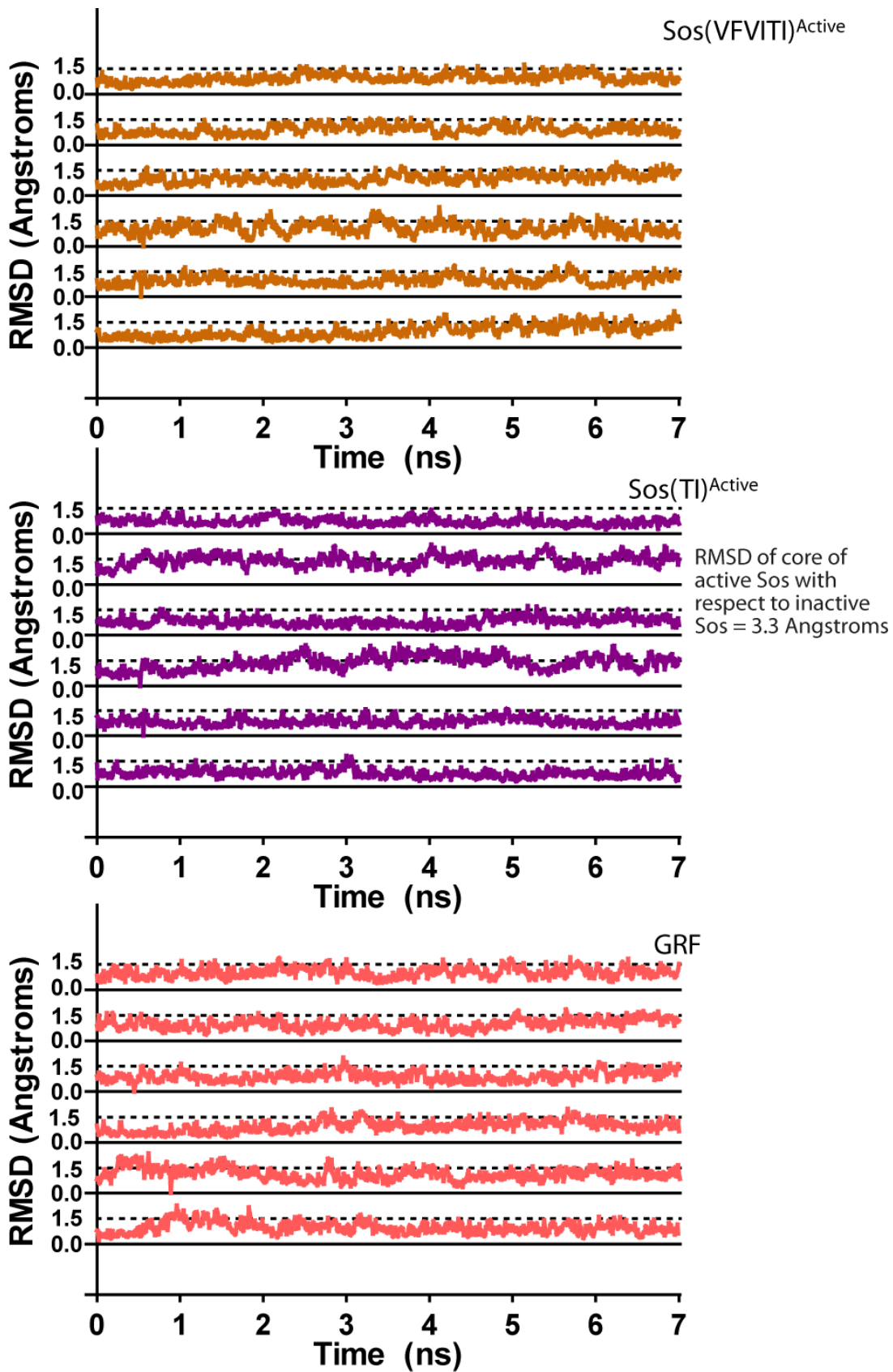


Supplementary Fig. 2. Ctd.

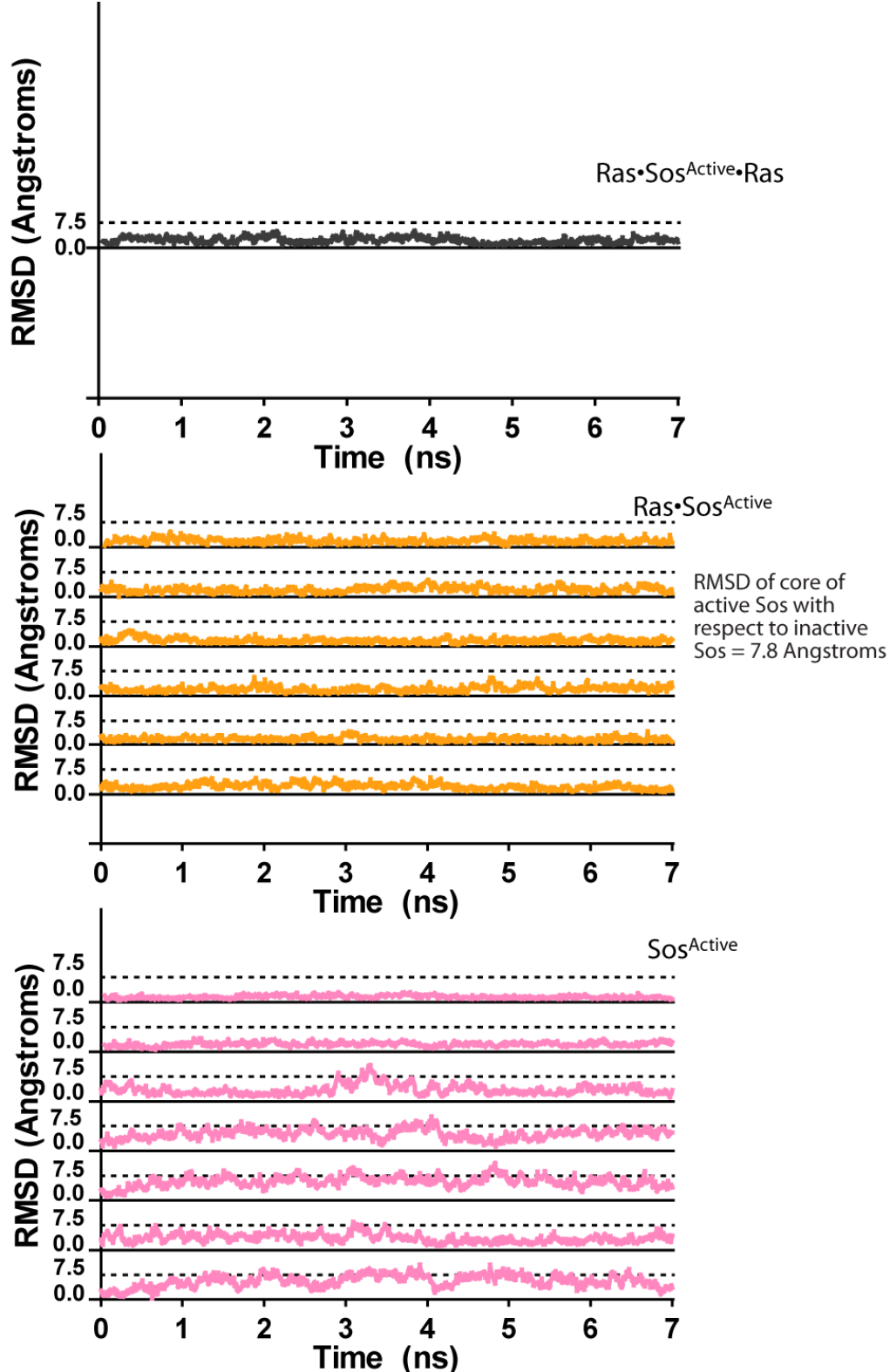


Supplementary Fig. 3. RMSD values of C_{α} residues in the helical hairpin with respect to the starting structure. Compare to **Supplementary Fig. 2.**

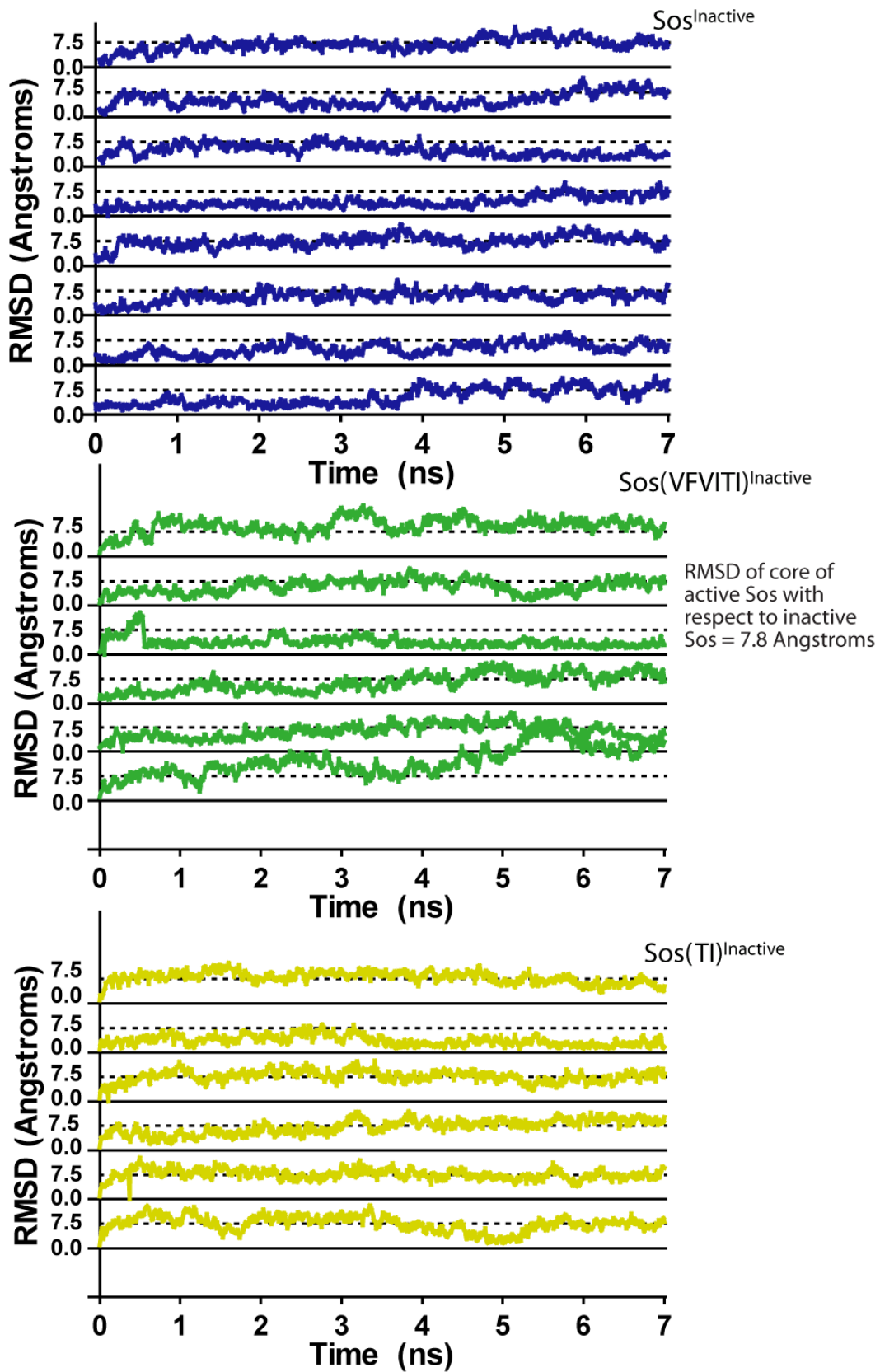
Continued on next page



Supplementary Fig. 3. Ctd.

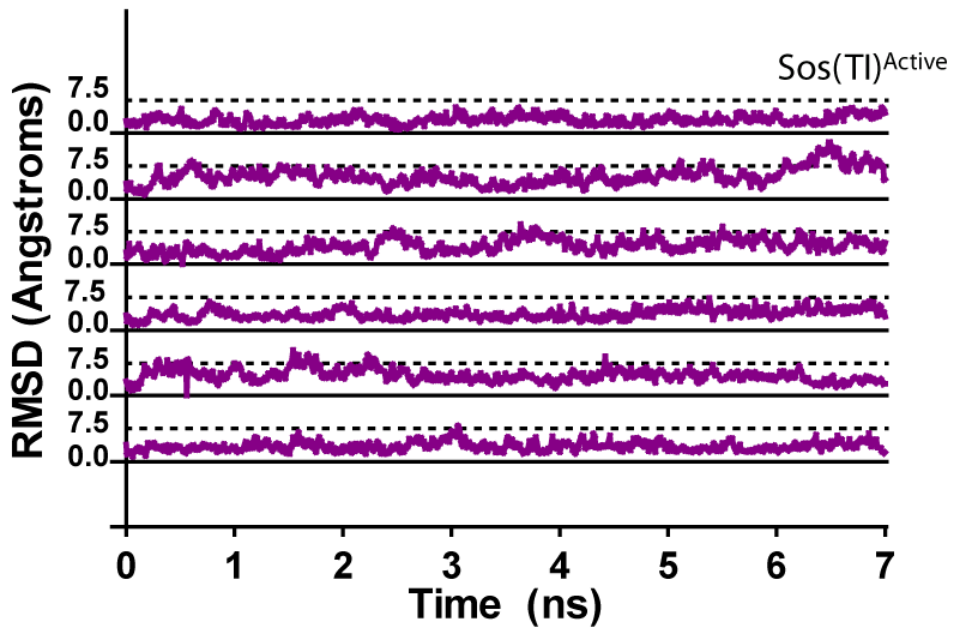
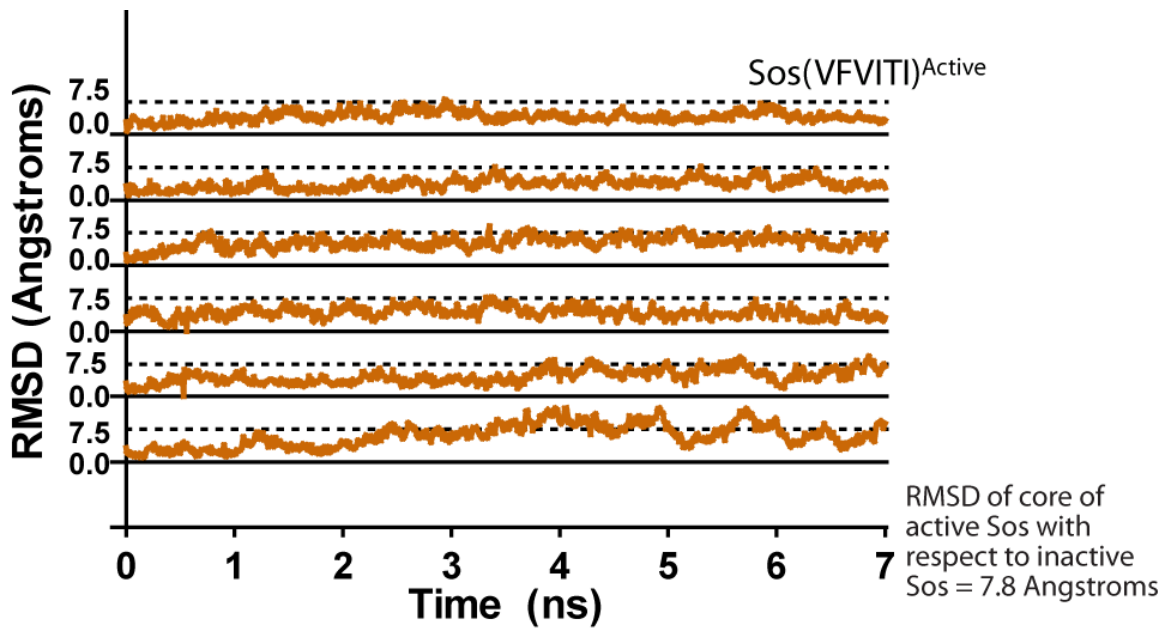


Supplementary Fig. 4. RMSD values of C_α residues in the Rem domain with respect to the starting structure. Replicates of the same simulation are shifted vertically by increments of 15 Å to facilitate visualization. Compare to **Supplementary Fig. 2** and **Supplementary Fig. 3**. Continued on next page

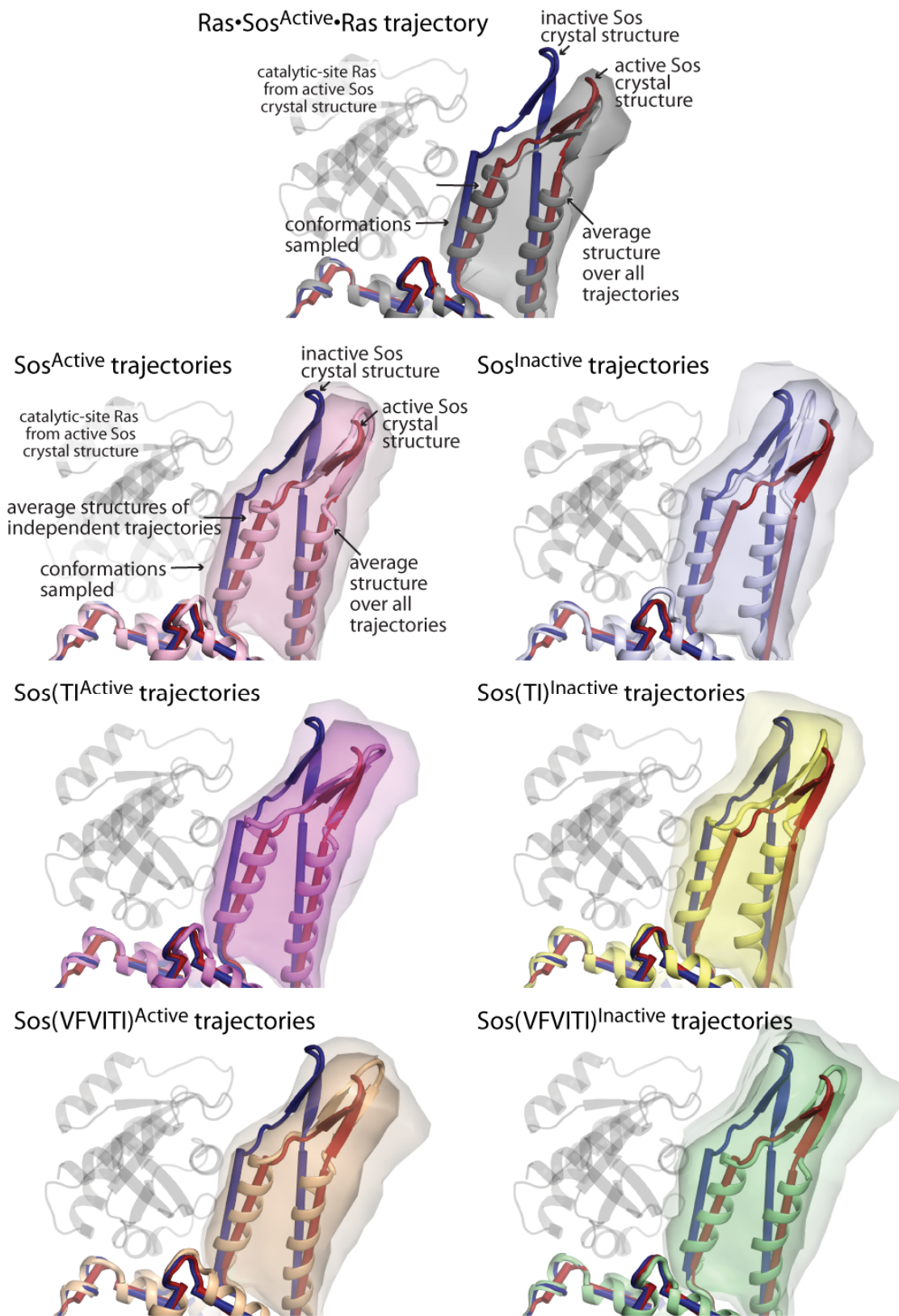


Supplementary Fig. 4. Ctd.

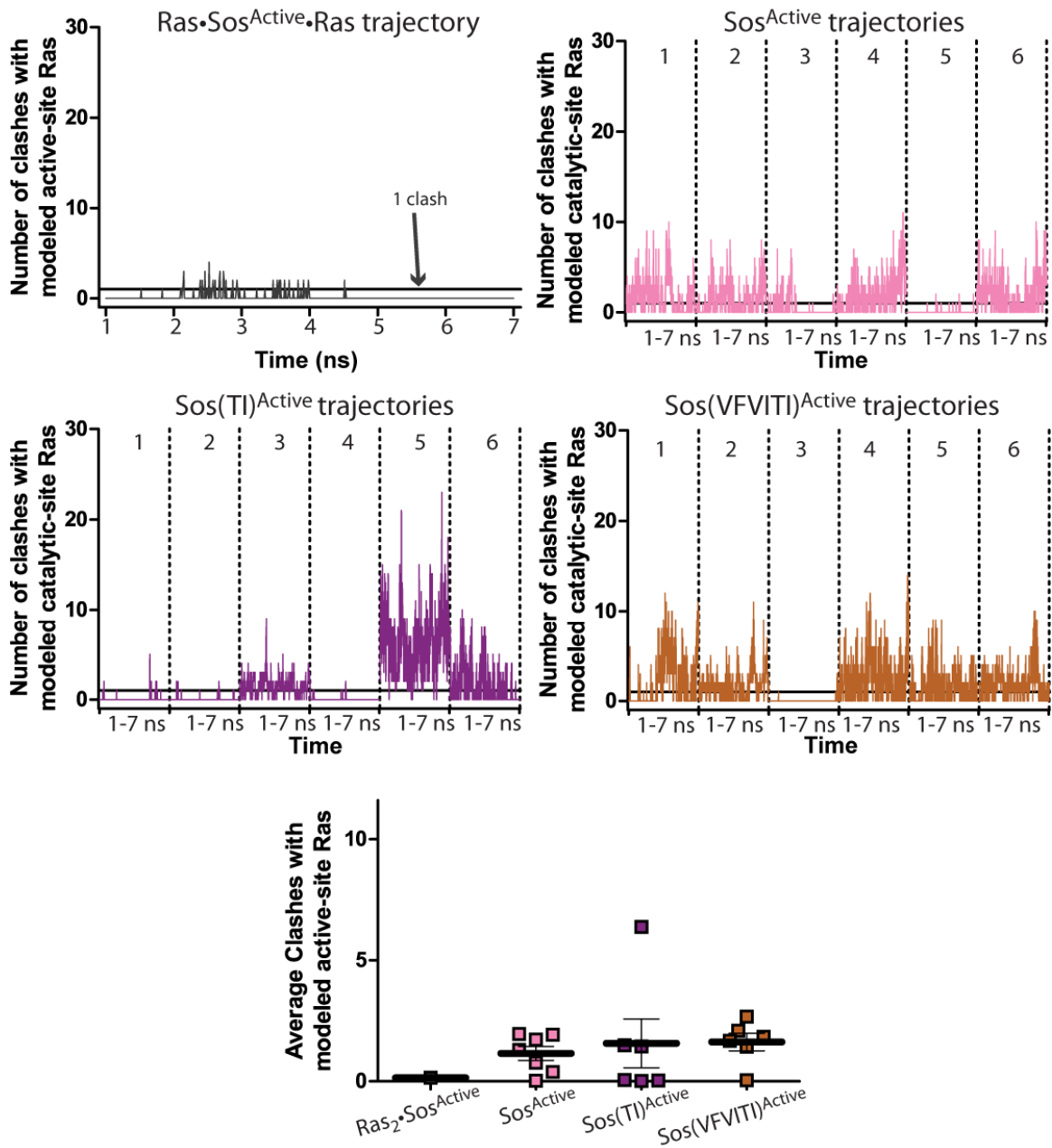
Continued on next page



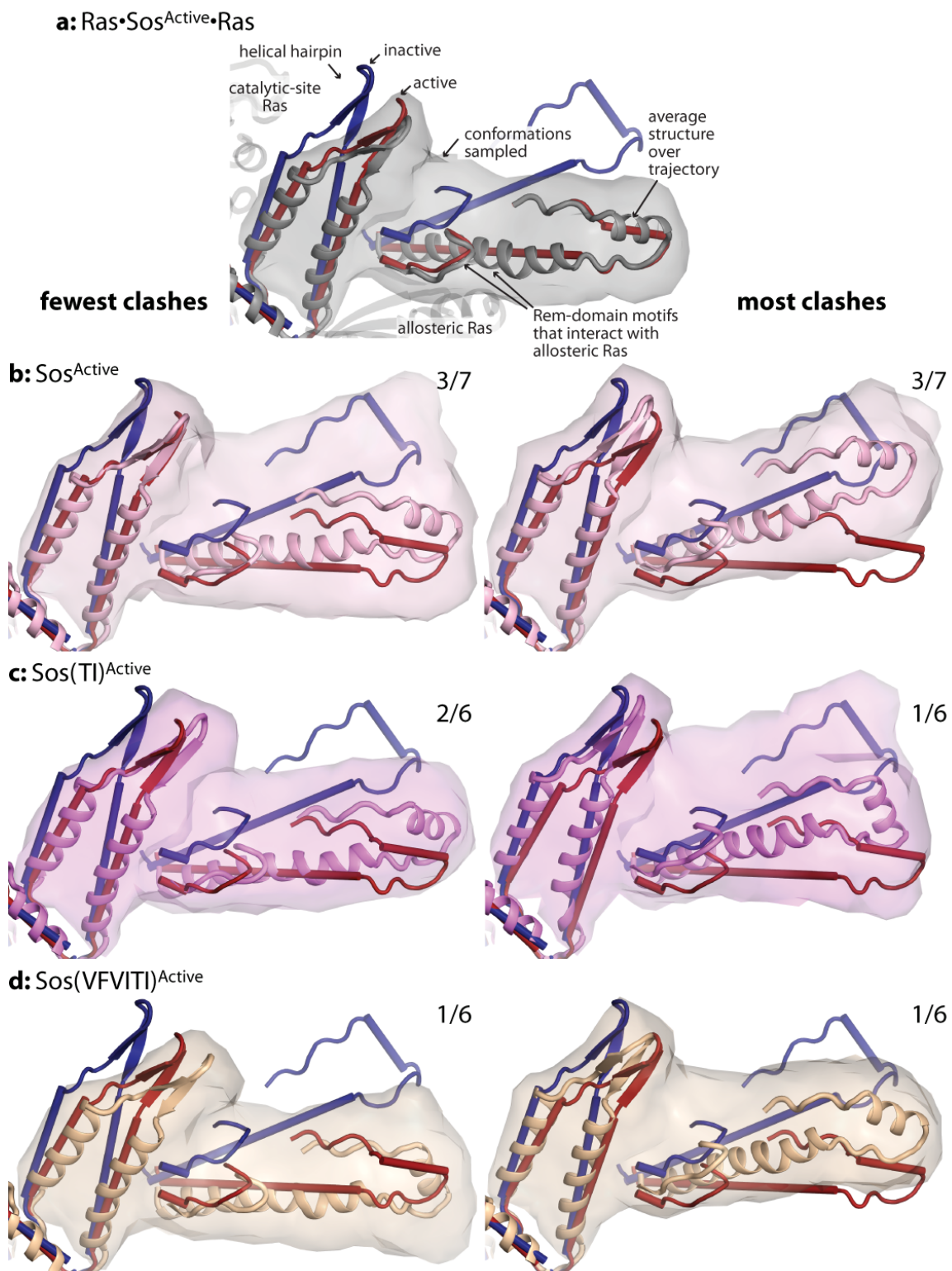
Supplementary Fig. 4. Ctd.



Supplementary Fig. 5. Conformation of the helical hairpin in molecular dynamics simulations of Sos. Compare with simulations in **Fig. 3**.

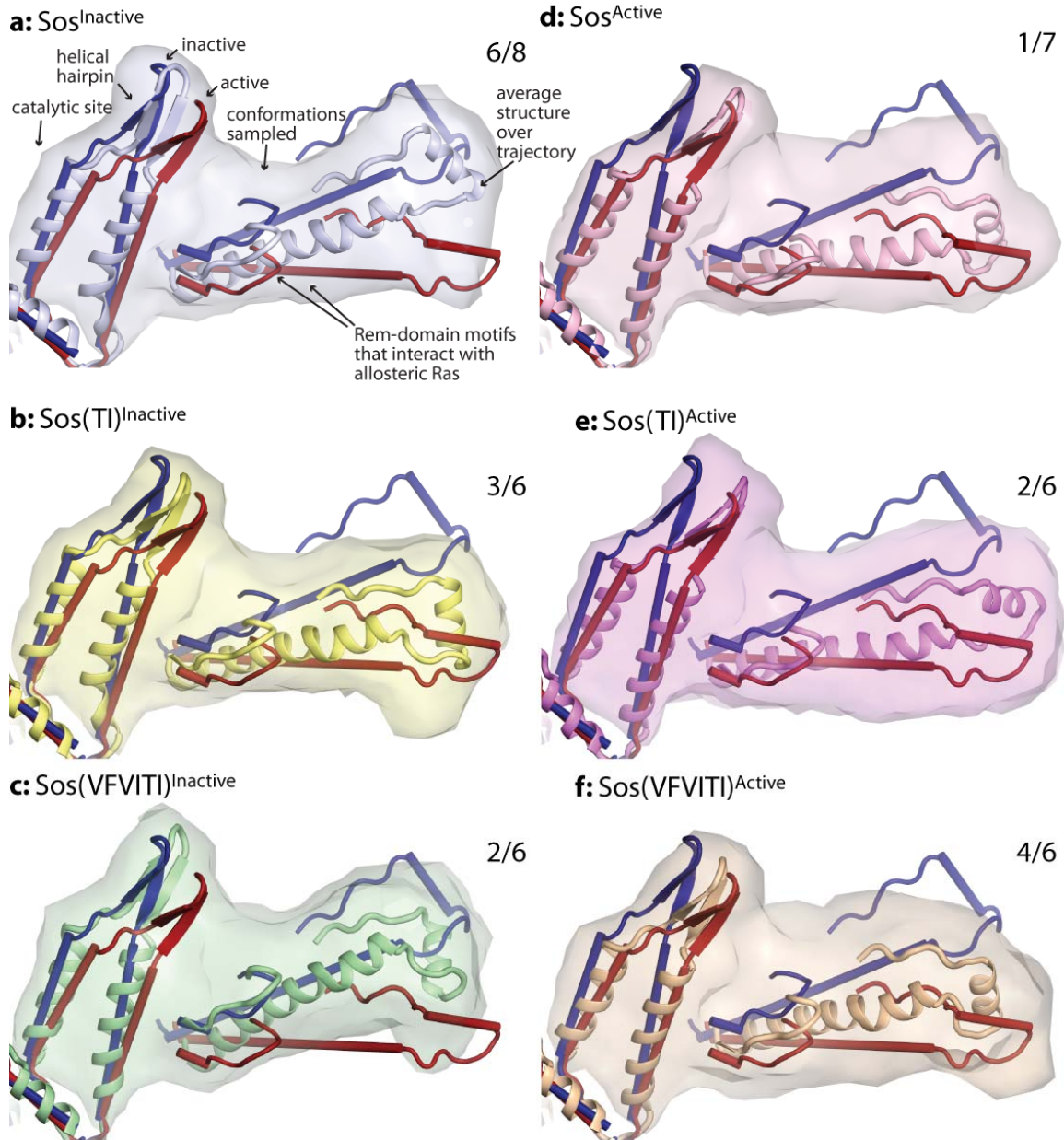


Supplementary Fig. 6. Active-site occlusion by the helical hairpin during simulations of Sos starting from the active conformation. Compare to Fig. 4.



Supplementary Fig. 7. Rem domain and helical hairpin conformations in simulations of Sos starting from the active conformation. Compare to **Fig. 5**.

intermediate number of clashes



Supplementary Fig. 8. Rem domain and helical hairpin conformations in simulations of Sos with intermediate numbers of clashes relative to others of the same type. Compare to **Fig. 5.** and **Supplementary Fig 7.**